

# Robust Nonlinear Control of a Variable-Pitch Quadrotor with the Flip Maneuver

Mahathi Bhargavapuri<sup>a</sup>, Soumya Ranjan Sahoo<sup>a</sup>, Mangal Kothari<sup>b,\*</sup>,  
Abhishek<sup>b</sup>

<sup>a</sup>*Dept. of Electrical Engineering, Indian Institute of Technology Kanpur, India*

<sup>b</sup>*Dept. of Aerospace Engineering, Indian Institute of Technology Kanpur, India*

---

## Abstract

This paper presents robust nonlinear control of a variable-pitch quadrotor with the flip maneuver. Backstepping approach is chosen for nonlinear control design. A control allocation loop dynamically computes the blade pitch angle of each rotor. A systematic method to select controller gains is presented that ensures closed-loop stability. Detailed analysis of the flip maneuver in the presence of input saturation is presented for the first time. Performance of the proposed control law is first verified through simulation. This is then implemented on a PixHawk open source autopilot board and flight tests are performed on an off-the-shelf variable-pitch quadrotor frame.

*Keywords:* Nonlinear Control; Backstepping Control; Quadrotor Dynamics; Variable-Pitch Actuation; Cascaded Systems.

---

## 1. Introduction

Quadrotors have been at the forefront of numerous applications involving unmanned aerial vehicles (UAVs). This is due to their immense mechanical simplicity as well as their ability to vertically take-off and land (VTOL). Defense applications such as surveillance, rescue, and reconnaissance are common for small UAVs with limited payload. However, an application like package delivery,

---

\*Corresponding author  
Email address: [mangal@iitk.ac.in](mailto:mangal@iitk.ac.in) (Mangal Kothari)

which is common in both civilian as well as defense scenario, requires higher payload carrying capabilities and hence larger UAVs.

Most large UAVs with the ability to hover are conventional helicopters with one main rotor and one tail rotor. These use only the main rotor for generating an upward thrust and tilts the tip path plane to achieve rolling and pitching moments. The upward thrust in such helicopters is generated by changing the collective pitch angle of the blades while rolling and pitching moments are achieved through cyclic inputs. This facilitates in increasing its flight envelope and control bandwidth but at the same time demands a complex actuation mechanism required to physically realize the cyclic inputs. To alleviate the problem of using a swash plate and an elaborate dynamical analysis, quadrotor helicopters are preferred. The mechanical simplicity of this design has inspired numerous works on modeling and control of a fixed-pitch quadrotor [1, 2, 3, 4]. Aggressive maneuvers and aerobatics of such quadrotors have been successfully demonstrated in [5, 6, 7, 8]. Yet, conventional quadrotors suffer from a few striking limitations: (a) the torque required to change the rotational speed of large motors in scaled up versions for larger payloads quickly becomes unattainable, and (b) fixed-pitch quadrotors are solely controlled by differential motor speeds, which implies control bandwidth is limited by rotor inertia. To overcome these shortcomings of a fixed-pitch quadrotor and still allow scaling up, the idea of using collective pitch controlled quadrotors is proposed. Use of variable-pitch propellers dramatically improves endurance and scalability, increases control bandwidth, and adds reverse thrust capabilities.

### *1.1. Background and Motivation*

A concerted effort towards the comparison of fixed- and variable-pitch actuators for small quadrotors along with linear control laws was done in [9, 10]. The authors have shown that rate of change of thrust is significantly higher with variable-pitch actuation. This difference in thrust rate is evident in larger quadrotors. The motor inertia limits the rate of change of thrust in conventional quadrotors to such an extent that it becomes impossible to maneuver and may

even lead to instability in the presence of external disturbances.

An improved flight dynamics model for a variable-pitch quadrotor was first introduced in [11]. The authors have utilized blade element theory (BET) with momentum theory (uniform inflow) to derive the rotor dynamics in terms of thrust coefficient. This reveals a nonlinear relationship between drag induced torque and the thrust coefficients used as virtual control inputs to the quadrotor. A control allocation loop was introduced to overcome this nonlinearity and dynamically allocate thrust and torque inputs to the thrust coefficients. However, this adds first order dynamics which has to be taken into account during the stability analysis. The present work addresses this issue by first designing a nonlinear backstepping controller which ensures the errors decay exponentially and the rate of decay can be explicitly decided by choosing the controller gains. By introducing a gain allocation methodology, the controller gains can be chosen such that the control allocation loop is stabilized at a much higher rate as compared to the attitude and position loops. This is analogous to the successive loop closure method of ensuring stability of cascaded systems. Other modeling errors are also taken care of without which successful experimental flights would not have been possible.

Various works focusing on efficient design, improved payload capabilities, and aerobatic maneuvers of variable-pitch quadrotors can be found in literature. Design and development of a gasoline powered unmanned variable-pitch quadrotor with PID based control has been carried out in [12], where the aim was to show higher endurance and efficient design utilizing a single power plant. Most of the work other than what has already been mentioned deals with design and modeling of variable-pitch quadrotors. Very few such works deal with control design and stability analysis for the new dynamic model. In [13], linear robust attitude controller is developed for this type of quadrotor. But results are restricted to stabilization of pitching moment of the vehicle. Motor speed control along with variable-pitch propellers are utilized in another related work with linear control laws where the focus is on finding the optimal combination of rotor speed control and collective pitch actuation to achieve either energy

efficient flight or to obtain the highest rate of change of thrust vector [14]. That being said, linear controllers are valid only while operating about hover condition. This can be seen in [15]. A single nonlinear control law is needed for the entire flight envelope which is not sensitive to noise and modeling uncertainties. Ample literature can be found on nonlinear control of fixed-pitch quadrotors. Early nonlinear control approaches such as dynamic inversion [16] and feedback linearization [17] lacked robustness. Other nonlinear control techniques like backstepping [18, 19, 20, 21], command-filtered backstepping [22], sliding mode [23, 24], geometric control [25], adaptive control [26, 27], event-triggered nonlinear control [28], and model predictive control with disturbance rejection [29] have been applied to fixed-pitch quadrotors with varying degrees of success. However, the dynamic control allocation required for a variable-pitch quadrotor implies that the aforementioned control laws cannot be directly applied without additional stability analysis and gain allocation. One might argue that a controller robust to input delays such as the one in [30, 31] can be used. But knowledge of the rotor dynamics and careful gain allocation along with a well tested nonlinear control law allows more flexibility when choosing the control technique. Existing works for missiles and conventional rotorcrafts that are robust to bounded uncertainties [32, 33], input saturation and delays with disturbance rejection [34] motivates the present work on robust nonlinear controllers for a variable-pitch quadrotor with a comprehensive analysis of the flip maneuver in the presence of input saturation. In [11], nonlinear dynamic inversion based control law was proposed for a variable-pitch quadrotor. But this did not contain proof that the proposed controller would remain stable with the inclusion of the control allocation loop. The control law also proved inefficient when experimentally tested due to its high sensitivity to modeling inaccuracies. To eliminate such drawbacks and still design a simple yet effective control law, backstepping methodology for control design is chosen. Robustness to modeling inaccuracies and bounded disturbances is also ensured by adding compensating terms to the nominal backstepping controller. Lyapunov-based stability analysis shows that the developed controllers are exponentially stable outside a compact

set with the errors remaining bounded for all time with only the bounds on the disturbances known *a priori*. Note that this work is the first to present the systematic design and validation of a nonlinear control law robust to uncertainties and bounded disturbances for the variable-pitch quadrotor. Control design with lesser information [35, 36, 37] and fault tolerant control [38, 39] for this novel vehicle present new set of challenges and are hence out of scope of the present work. These works, however, provide interesting future research directions on the variable-pitch platform. Some of the main contributions of this work are highlighted in the next section.

### 1.2. Contributions

To ensure stability and tracking over the full flight envelope of the vehicle and retain design simplicity in the presence of modeling uncertainties and disturbances, robust backstepping technique is chosen for Lyapunov-based nonlinear control design. The contributions of this work can be briefly enumerated as follows:

- Nominal backstepping control laws for the attitude and position subsystems is designed analogous to conventional quadrotors. The design of such backstepping controllers is, in general, subject to some basic restrictions and assumptions [18, 20]. However, the flight envelope and the rotor dynamics of a variable-pitch quadrotor is significantly different from that of a conventional quadrotor. Hence, a distinct set of restrictions on the developed control law is provided for the new type of quadrotor helicopter.
- The additional dynamics of the control allocation loop are taken into account to ensure stability of the full system. Three nested loops are considered: the outer or position control loop, the intermediate or attitude control loop, and the innermost or the control allocation loop. The time-scale separation between these three loops is utilized to choose controller gains in a systematic way such that the full system is exponentially stable.

- To ensure that the errors remain bounded in the presence of modeling uncertainties and bounded disturbances, it is proposed that a robust compensation term be added to the nominal backstepping control law. Rigorous stability proof is provided which give explicit bounds on the errors.
- The flip maneuver, that only quadrotors with variable-pitch actuation can achieve, is analyzed in the presence of input saturation. Such a thorough analysis of the maneuver has hitherto not been done. It sheds light on the loss of height during the transition from normal to inverted flight mode (and vice versa) that cannot be avoided while input saturation exists. Theoretical results provide the set of roll angle values for which altitude control is lost along with the time period within which control is regained. Numerical simulations describe altitude subsystem during this maneuver while real-time experiments show that the attitude controller ensures correlation with theoretically predicted behavior in terms of time spent in regions of the flight envelope with no altitude control.
- Thorough simulation and experimental comparisons between the proposed robust nonlinear controller and PID is presented to highlight the improved tracking performance.
- A detailed description of experimental flights using an off-the-shelf frame and the proposed nonlinear control law is given for the first time.

The rest of the paper is organized as follows: A mathematical model for a variable-pitch quadrotor is discussed in Section 2. Nominal and robust nonlinear backstepping controllers are developed in Section 3 along with flip maneuver analysis and the dynamic control allocation loop. Design of the nominal control laws leads to a systematic way to choose controller gains. Simulation and experiments showing attitude and position tracking as well as flipping are presented in Sections 4 and 5. Concluding remarks are given in Section 6.

## 2. Rotor and Rigid-Body Dynamics

Rigid-body dynamics of the variable-pitch quadrotor is derived using Newton-Euler equations similar to that of conventional quadrotors [18, 40]. However, the similarities end there. Since the mechanism for regulating thrust and torque of each rotor is significantly different in a variable-pitch quadrotor, rotor dynamics have to be analyzed separately. This was done previously in [11] but had a few shortcomings. Whilst there are similarities between the two models, significant differences can be observed when it comes to control design. These distinctions become discernible in the subsequent sections on control design and control allocation.

### 2.1. Rigid-body Dynamics

Translational and rotational dynamics of the quadrotor are derived in this section using linear and angular momentum conservation laws. First, inertial and body-fixed frames of reference are defined as shown in Fig. 1. The subscripts I and b indicate inertial and body-fixed frames, respectively. Combined thrust produced by the four rotors and the force of gravity are considered to be the dominant forces acting on the quadrotor. Aerodynamic forces on the airframe are not examined since their effect on the overall flight dynamics is not significant. The translational dynamics in inertial frame can be written as

$$\begin{pmatrix} \ddot{x} \\ \ddot{y} \\ \ddot{z} \end{pmatrix} = \begin{pmatrix} c\theta c\psi & s\phi s\theta c\psi - c\phi s\psi & c\phi s\theta c\psi + s\phi s\psi \\ c\theta s\psi & s\phi s\theta s\psi + c\phi c\psi & c\phi s\theta s\psi - s\phi c\psi \\ -s\theta & s\phi c\theta & c\phi c\theta \end{pmatrix} \begin{pmatrix} 0 \\ 0 \\ \frac{-U_1}{m} \end{pmatrix} + \begin{pmatrix} 0 \\ 0 \\ g \end{pmatrix} \quad (1)$$

The rotation matrix relating the body frame to the inertial frame of reference is formed by Euler angles ( $\phi$  - roll,  $\theta$  - pitch, and  $\psi$  - yaw, in that sequence). Here,  $(x, y, z)^T$  is the quadrotor position in the inertial frame,  $m$  is the quadrotor mass, and  $g$  is the acceleration due to gravity.  $U_1$  is the total thrust generated by all four rotors combined and acts along  $z_b$ -axis. Cosine and sine functions are denoted by  $c(\cdot) := \cos(\cdot)$  and  $s(\cdot) := \sin(\cdot)$ , respectively.

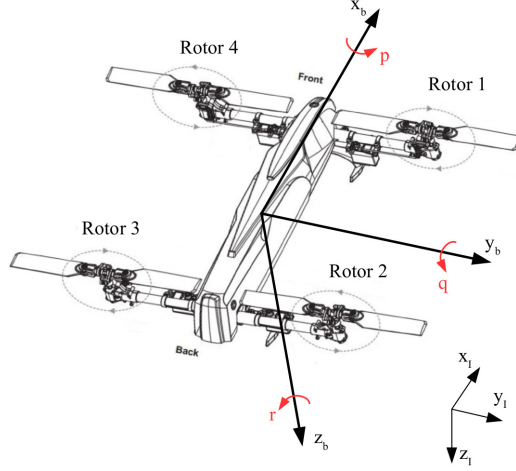


**Figure 1:** Variable-pitch quadrotor

Attitude of the variable-pitch quadrotor is defined in terms of Euler angles. The Euler angles are defined in three different frames of reference and the angular rates ( $p, q, r$ ) are defined in the body frame [41]. The kinematics and dynamics of rotational motion are given by

$$\begin{pmatrix} \dot{\phi} \\ \dot{\theta} \\ \dot{\psi} \end{pmatrix} = \begin{pmatrix} 1 & \sin \phi \tan \theta & \cos \phi \tan \theta \\ 0 & \cos \phi & -\sin \phi \\ 0 & \sin \phi \sec \theta & \cos \phi \sec \theta \end{pmatrix} \begin{pmatrix} p \\ q \\ r \end{pmatrix} \quad (2)$$

$$\begin{pmatrix} \dot{p} \\ \dot{q} \\ \dot{r} \end{pmatrix} = \begin{pmatrix} \frac{I_{yy}-I_{zz}}{I_{xx}} qr \\ \frac{I_{zz}-I_{xx}}{I_{yy}} pr \\ \frac{I_{xx}-I_{yy}}{I_{zz}} pq \end{pmatrix} + \begin{pmatrix} \frac{U_2}{I_{xx}} \\ \frac{U_3}{I_{yy}} \\ \frac{U_4}{I_{zz}} \end{pmatrix} \quad (3)$$

where  $I_{xx}$ ,  $I_{yy}$ ,  $I_{zz}$  are the moments of inertia about  $x_b$ -,  $y_b$ -,  $z_b$ -axes, respectively. The product of inertia terms are assumed to be negligible since the quadrotor is symmetric about its  $x_b$ - and  $y_b$ -axes.  $U_2$ ,  $U_3$ , and  $U_4$  are the externally applied rolling, pitching, and yawing moments in the body-fixed frame, respectively. These moment inputs are generated due to change in collective pitch angle of the propellers. The control inputs  $U_1$ ,  $U_2$ ,  $U_3$ , and  $U_4$  are now in terms of thrust coefficients which are directly related to blade pitch angle of the

propellers. These can be derived using momentum theory and blade element theory and is discussed in detail in the next section.

## 2.2. Rotor Dynamics

Unlike a conventional quadrotor, the thrust produced by a variable-pitch quadrotor is varied by changing collective pitch of the rotor blades. Momentum theory and Blade Element Theory (BET) are used to calculate the thrust and torque from each rotor as a function of its thrust coefficient [42].

The principles of BET assume that each blade is divided cross-sectionally into 2-D airfoils which do not have any mutual influence on each other. The contribution of each blade element to the total air load (lift, drag, and pitching moment) is calculated and integrated over the blade radius to arrive at the total thrust and torque generated by each rotor. The relationship between thrust coefficient,  $C_T$ , and pitch angle,  $\theta_0$ , for an untwisted blade with uniform inflow [42] is given by

$$C_T = \frac{1}{2}\sigma C_{l_\alpha} \left( \frac{\theta_0}{3} - \frac{\lambda}{2} \right) \quad (4)$$

where  $\sigma = \frac{N_b c}{\pi R}$  is the solidity ratio,  $N_b$  is the number of blades in the rotor,  $c$  is the chord length of the rotor,  $R$  is rotor radius, and  $C_{l_\alpha}$  is the airfoil lift curve slope.

Assumption for uniform inflow is made to ensure simplicity of model for control design. The non-uniform inflow models such as dynamic inflow or prescribed wake models are computationally expensive and iterative in nature. One such advanced model for variable-pitch quadrotors can be found in [43]. This does not assume uniform inflow and utilizes Blade Element Momentum Theory (BEMT) to iteratively compute thrust and torque coefficients. A quick comparison between the values of  $C_T$  computed using (4) and the method in [43] shows that the error introduced due to the uniform inflow assumption is minimal. Also, this error can be treated as unmodeled dynamics and represented as a lumped uncertainty for each rotor model. A fairly accurate model along with some uncertainty motivates robust control design which is implementable in real-time and ensures boundedness of tracking error.

Using momentum theory for hover condition, inflow ratio,  $\lambda$ , can be expressed as

$$\lambda = \sqrt{\frac{C_T}{2}} \quad (5)$$

Therefore, the collective pitch input to the rotor comes out to be

$$\theta_0 = \frac{6C_T}{\sigma C_{l_\alpha}} + \frac{3}{2} \sqrt{\frac{C_T}{2}} \quad (6)$$

The torque coefficient for each rotor is derived using BET in a similar fashion [42] and is given by

$$C_Q = \frac{1}{2} \sigma \left( \frac{\sqrt{2} C_T^{\frac{3}{2}}}{\sigma} + \frac{C_{d_0}}{4} \right) \quad (7)$$

where  $C_{d_0}$  is the zero lift drag coefficient of the airfoil. Thrust and torque for the  $i^{\text{th}}$  rotor are given by

$$T_i = KC_{T_i} \quad (8)$$

$$Q_i = KRC_{Q_i} \quad (9)$$

where  $K = \rho\pi R^2 V_{tip}^2$ ,  $\rho$  is the density of air,  $V_{tip} = \Omega R$ , and  $\Omega$  is angular speed of the rotor.  $K$  is typically a constant since  $\Omega$  is regulated about a constant value. Thus, the total thrust for a quadrotor is given by

$$U_1 = \gamma (C_{T_1} + C_{T_2} + C_{T_3} + C_{T_4}) \quad (10)$$

In practice, the total thrust of any vehicle cannot increase or decrease indefinitely. Hence, an input saturation given by design constraints is imposed on  $U_1$ . Rotor crafts are typically designed to produce a maximum thrust that is twice their weight. This limit becomes both mathematically and physically significant while developing the control law and analyzing the flip maneuver. A decision variable  $\gamma$  is introduced to command the vehicle to flip and utilize its reverse thrust capabilities. This is defined as

$$\gamma = \begin{cases} 1, & \text{for normal mode} \\ -1, & \text{for inverted mode} \end{cases} \quad (11)$$

When the quadrotor is required to flip,  $\gamma$  is set to -1. This is also used to alter the commanded roll and pitch angles during inverted flight which shall be discussed in the control design section.

The control inputs  $U_2$ ,  $U_3$ , and  $U_4$  are derived next in terms of the thrust coefficients. Similar to fixed-pitch quadrotors, positive roll of a variable-pitch quadrotor in H-configuration (see Fig. 1) can be achieved by providing higher thrust to rotors 3 and 4, and correspondingly lower thrust to rotors 1 and 2. Positive pitch of the vehicle can be achieved by providing higher thrust to rotors 1 and 4, and correspondingly lower thrust to rotors 2 and 3. As a result of the drag force acting on each rotor, torques produced by rotors 2 and 4 are along the positive  $z_b$ -axis and torques produced by rotors 1 and 3 are along the opposite direction. A non-zero net torque along the  $z_b$ -axis causes yawing motion. Equations (12)-(14) give the control inputs for roll, pitch, and yaw moments, respectively.

$$U_2 = \gamma d K (-C_{T_1} - C_{T_2} + C_{T_3} + C_{T_4}) \quad (12)$$

$$U_3 = \gamma d K (C_{T_1} - C_{T_2} - C_{T_3} + C_{T_4}) \quad (13)$$

$$U_4 = \frac{KR}{\sqrt{2}} \left( -|C_{T_1}|^{\frac{3}{2}} + |C_{T_2}|^{\frac{3}{2}} - |C_{T_3}|^{\frac{3}{2}} + |C_{T_4}|^{\frac{3}{2}} \right) \quad (14)$$

Here  $d$  is the distance between the rotor axis and the vehicle's centre of gravity. It is clear from (14) that the relationship between yawing moment and thrust coefficients is nonlinear. To tackle this nonlinearity, a dynamic control allocation loop is introduced. This makes control design and the associated stability analysis challenging and will be seen in the coming sections.

### 3. Control Design

In this section, a nonlinear controller along with dynamic control allocation for a variable-pitch quadrotor is developed. To keep the design of a nonlinear control law simple and elegant while being able to consider the nonlinearities of the model to perform aggressive maneuvers, backstepping methodology is chosen. This also provides scope to add robustness to modeling uncertainties

and bounded disturbances. One of the main challenges of implementing nonlinear control laws on a variable-pitch quadrotor is the nonlinear relationship between the thrust coefficients and the moment input as shown in (14) which necessitates the use of a dynamic control allocation loop. Since such a control allocation methodology adds a first order dynamics of its own, the present work intends to study the effect of utilizing such a control allocation scheme on the overall stability of the vehicle.

At the outset, working of the dynamic control allocation is described, since it is essential to ensure that appropriate signals are generated for the actuators. The control allocation loop takes the control signals generated by the position and attitude controllers as the desired value of the actual control inputs given in (10)-(14). Thrust coefficients and their derivatives are used as virtual controls to design a dynamic control allocation loop. Blade pitch angles are then computed using the thrust coefficient values. These collective pitch angle values are used as actuating signals for the servos on the quadrotor.

The objective of the proposed controller is to track the inertial position states ( $x, y, z$ ) and the vehicle's heading  $\psi$ . Four states are chosen to be controlled as only four control inputs are available. The commanded variables  $x$  and  $y$  cannot be directly controlled due to the nature of the available control inputs. These variables are controlled by choosing appropriate  $\phi$  and  $\theta$ . Hence, a backstepping controller for motion in  $x_I-y_I$  plane is developed which generates the desired roll and pitch angles for both normal and inverted flight modes. The attitude controller then computes the required moments to generate the desired roll and pitch angles along with the desired heading ( $\psi$ ). An altitude controller is developed to ensure exponential tracking within the given saturation bounds. Finally, a detailed analysis of the flip maneuver is presented.

The stability properties of the overall closed-loop system is analyzed next. To preserve the cascade structure of the full system resulting from time-scale separation principles, the dynamics of the control allocation loop have to be fast enough to ensure that the thrust coefficients computed by this loop reach their steady state values before the control signal set points change. This is a unique

aspect of variable-pitch quadrotors and has to be analyzed separately. This paper provides a method to decide the controller gains systematically and hence ensure that the cascade structure of the position, attitude, and control allocation loops is preserved. Section 3.6 explains how adding a robust compensation term to the nominal backstepping control law ensures boundedness of errors in the presence of uncertainties and disturbances. This completes the control design for a variable-pitch quadrotor.

### 3.1. Control Allocation

The position and attitude controllers in Sections 3.3 and 3.6 provide the desired values of control inputs  $U_i$  ( $i = 1,2,3,4$ ). The actual controls in (10)-(14) however cannot be directly mapped as in the case of conventional quadrotors, since the equation governing yawing moment is nonlinear. The nonlinear nature of the control inputs in (10)-(14) necessitates the use of dynamic control allocation where thrust coefficients are used as virtual controls. These coefficients are obtained by first computing thrust coefficient derivatives and integrating its result. The corresponding blade pitch angles are then computed using (6). To ensure simple computation of thrust coefficient derivatives via control input derivatives, stable first-order dynamics are introduced given by

$$\dot{U}_i = k_i(U_{id} - U_i), \quad k_i > 0, \quad (15)$$

This represents stable first order error dynamics for the error  $E_i = U_i - U_{id}$  with  $\dot{U}_{id} = 0$  which forces  $U_i$  to follow  $U_{id}$ . Here,  $U_{id}$  is obtained from the position and attitude control laws. The value of  $U_i$  is calculated dynamically using (10)-(14), where  $C_{T_i}$  is initialized to the theoretical value at hover. Next,  $\dot{U}_i$  is utilized to calculate derivatives of thrust coefficients from the expression

$$\begin{pmatrix} \dot{C}_{T_1} \\ \dot{C}_{T_2} \\ \dot{C}_{T_3} \\ \dot{C}_{T_4} \end{pmatrix} = M^{-1} \begin{pmatrix} \dot{U}_1 \\ \dot{U}_2 \\ \dot{U}_3 \\ \dot{U}_4 \end{pmatrix} \quad (16)$$

where

$$M = \begin{pmatrix} \gamma K & \gamma K & \gamma K & \gamma K \\ -\gamma dK & -\gamma dK & \gamma dK & \gamma dK \\ \gamma dK & -\gamma dK & -\gamma dK & \gamma dK \\ -\frac{3KR}{2} \left( \frac{|C_{T_1}|}{2} \right)^{\frac{1}{2}} & \frac{3KR}{2} \left( \frac{|C_{T_2}|}{2} \right)^{\frac{1}{2}} & -\frac{3KR}{2} \left( \frac{|C_{T_3}|}{2} \right)^{\frac{1}{2}} & \frac{3KR}{2} \left( \frac{|C_{T_4}|}{2} \right)^{\frac{1}{2}} \end{pmatrix}$$

The blade pitch angles computed from thrust coefficients are converted to pulse-width modulated (PWM) signals for the servos. The servos act as the actuators for changing the collective blade pitch angles. The  $U_i$ 's in (15) are updated for the next time instant using these new  $C_{T_i}$ 's along with the  $U_{id}$ 's from the control laws at the next time instant.

The  $k_i$ 's in (15) have to be chosen such that the control allocation loop evolves at a rate that is 5-10 times higher than both altitude and attitude closed-loop systems. This means that the steady state values of the collective pitch angles have to be reached well before any change in  $U_{id}$  occurs. This ensures that  $U_i \approx U_{id}$  is satisfied which validates the Lyapunov stability analysis provided for the developed control laws.

### 3.2. State-Space Representation

For the purpose of control design using backstepping approach, the quadrotor model is represented in state space domain which has a strict feedback structure. State vectors  $x_1$ ,  $x_2$  contain Euler angles ( $\phi$ -roll,  $\theta$ -pitch,  $\psi$ -yaw) and body angular rates ( $p$ ,  $q$ ,  $r$ ), respectively. The inertial position of the vehicle is broken into states  $x_3$  and  $x_5$ , as given in (17). The corresponding velocities in inertial frame are defined by states  $x_4$  and  $x_6$ .

$$x_1 = \begin{pmatrix} \phi \\ \theta \\ \psi \end{pmatrix}, x_2 = \begin{pmatrix} p \\ q \\ r \end{pmatrix}, x_3 = z, x_4 = \dot{z}, x_5 = \begin{pmatrix} x \\ y \end{pmatrix}, x_6 = \begin{pmatrix} \dot{x} \\ \dot{y} \end{pmatrix} \quad (17)$$

The nonlinear dynamical system in (1)-(3) can be represented as a combination of three subsystems. The first subsystem,  $S_R$ , represents the rotational dynamics of the vehicle as given in (19). Product of inertia terms are assumed to be

negligible. The second subsystem,  $S_A$ , given by (20) represents the altitude dynamics of the vehicle. The last subsystem,  $S_H$ , represents the horizontal plane dynamics of the vehicle and is given by (21). However, the rigid body dynamics given by (1) and (3) do not entirely encapsulate the behavior of the variable-pitch quadrotor, especially during aggressive maneuvers which can introduce aerodynamic forces and disturbances. These uncertainties and disturbances experienced by the  $S_R$ ,  $S_A$ , and  $S_H$  subsystems are represented in (19)-(21) by  $\Delta_R \in \mathbb{R}^3$ ,  $\Delta_A \in \mathbb{R}$ , and  $\Delta_H \in \mathbb{R}^2$ , respectively. These uncertainties and disturbances are with their bounds given by

$$\|\Delta_R\|_\infty \leq \delta_R, \quad \|\Delta_A\|_\infty \leq \delta_A, \quad \|\Delta_H\|_\infty \leq \delta_H, \quad (18)$$

where  $\|\cdot\|_\infty$  denotes the infinity norm defined on the Euclidean space of appropriate dimension, and  $\delta_R$ ,  $\delta_A$ , and  $\delta_H$  are real positive constants.

$$S_R : \begin{cases} \dot{x}_1 = \underbrace{\begin{pmatrix} 1 & \sin \phi \tan \theta & \cos \phi \tan \theta \\ 0 & \cos \phi & -\sin \phi \\ 0 & \sin \phi \sec \theta & \cos \phi \sec \theta \end{pmatrix}}_{g_0} x_2 \\ \dot{x}_2 = \underbrace{\begin{pmatrix} \frac{(I_{yy}-I_{zz})}{I_{xx}} qr \\ \frac{(I_{zz}-I_{xx})}{I_{yy}} pr \\ \frac{(I_{xx}-I_{yy})}{I_{zz}} pq \end{pmatrix}}_{f_1} + \underbrace{\begin{pmatrix} \frac{1}{I_{xx}} & 0 & 0 \\ 0 & \frac{1}{I_{yy}} & 0 \\ 0 & 0 & \frac{1}{I_{zz}} \end{pmatrix}}_{g_1} \begin{pmatrix} U_2 \\ U_3 \\ U_4 \end{pmatrix} + \Delta_R \end{cases} \quad (19)$$

$$S_A : \begin{cases} \dot{x}_3 = x_4 \\ \dot{x}_4 = \underbrace{g}_{f_2} - \underbrace{\frac{\cos \phi \cos \theta}{m}}_{g_2} U_1 + \Delta_A \end{cases} \quad (20)$$

$$S_H : \begin{cases} \dot{x}_5 = x_6 \\ \dot{x}_6 = \underbrace{\frac{-U_1}{m} \begin{pmatrix} \sin \psi & \cos \psi \\ -\cos \psi & \sin \psi \end{pmatrix}}_{g_3} \underbrace{\begin{pmatrix} \sin \phi \\ \cos \phi \sin \theta \end{pmatrix}}_{\bar{u}} + \Delta_H \end{cases} \quad (21)$$

The system is divided into three subsystems depending on whether they have an actual control input available or not. The subsystems  $S_A$  and  $S_R$  have real inputs  $U_1$ ,  $U_2$ ,  $U_3$ , and  $U_4$ , whereas the angles  $\phi$  and  $\theta$  act as virtual inputs to the  $S_H$  subsystem. Since these subsystems are individually in strict feedback form, backstepping technique becomes an intelligible choice for control design.

The unmodeled dynamics in (4) and (7) as well as the disturbances encountered by the vehicle during flight have to be taken into account for the purpose control design. Nominal backstepping cannot ensure bounded errors when such uncertainties are present. Hence, robust backstepping is proposed in Section 3.6 to ensure tracking errors remain bounded. However, due to the presence of the control allocation loop, robust controller gains have to be chosen carefully to ensure stability of the overall closed-loop system. In order to systematically decide controller gains, the uncertainties  $\Delta_R$ ,  $\Delta_A$ , and  $\Delta_H$  are neglected and nominal backstepping control laws are first designed. Then, gain allocation based on the exponential stability properties of nominal backstepping controllers is presented in Section 3.5. Finally, robustness terms are added to the nominal backstepping control laws in Section 3.6 to ensure tracking errors are uniformly bounded in the presence of  $\Delta_R$ ,  $\Delta_A$ , and  $\Delta_H$ .

**Remark 1.** *Backstepping control design requires the inversion of the functions  $g_0$ ,  $g_1$ ,  $g_2$ , and  $g_3$ . The diagonal inertia matrix  $g_1$  is clearly invertible. The function  $g_3$  is invertible since its determinant is  $(\frac{U_1}{m})^2$  and the thrust input  $U_1$  is always a finite, non-zero value while in flight and does not go to zero during flipping as well. Physical systems cannot produce arbitrarily large control inputs. Hence, the maximum total thrust  $U_1$  is restricted to  $2mg$  for the vehicle in consideration. This restriction is numerically reflected in the saturation on  $U_{1d}$  (used for altitude control design) which ensures that the control input remains bounded when it passes through the singular points of  $g_2$ . The thrust input  $U_1$  is responsible for both counteracting the gravitational force along the  $z_1$ -axis as well as provide horizontal acceleration for trajectory tracking in the  $x_1$ - $y_1$  plane. To ensure altitude control is not lost while performing maneuvers in the  $x_1$ - $y_1$  plane,*

the desired roll and pitch angles are restricted to the interval  $(-\frac{\pi}{3}, \frac{\pi}{3}) \cup (-\frac{2\pi}{3}, \frac{2\pi}{3})$  for normal and inverted flight. This also defines the flight envelope of the vehicle as the regions where stability and tracking of the position states  $(x, y, z)$  and the heading  $\psi$  is guaranteed. The restriction on roll and pitch angles also implicitly ensures invertibility of the function  $g_0$ . Note that during a flip, altitude control is lost momentarily. During the flip maneuver, the states  $\phi$  and  $\theta$  are stabilized instead of the horizontal position states  $x$  and  $y$ . A thorough analysis is provided in Section 3.4.

**Remark 2.** Imposing a saturation on the total thrust,  $U_1$ , implicitly places saturations on the moment inputs  $U_2$ ,  $U_3$ , and  $U_4$ . Knowing the value of input saturation of  $U_1$ , hence, enables computation of the remaining saturation values. However, these are not vital for the stability analysis of the closed-loop system or the flip maneuver which is unique to variable-pitch quadrotors. Simulation studies may be carried out to confirm that the inputs  $U_2$ ,  $U_3$ , and  $U_4$  are well within their saturation limits over the full flight envelope.

### 3.3. Position and Attitude Control

The desired position  $(x_d, y_d, z_d)$  and the desired heading  $\psi_d$  are the commanded inputs to the vehicle controller. The subscript  $d$  stands for desired value of the states. As mentioned earlier, the angles  $\phi$  and  $\theta$  act as virtual inputs to the subsystem  $S_H$ . Hence, the commanded variables are first transformed from  $(x_d, y_d, z_d, \psi_d)$  to  $(\phi_d, \theta_d, z_d, \psi_d)$ . Thus, a backstepping control law is derived for the  $S_H$  subsystem first. Next, the attitude controller uses the desired Euler angles  $(\phi_d, \theta_d, \psi_d)$  to generate the required moment inputs  $U_{2d}$ ,  $U_{3d}$ , and  $U_{4d}$ . Finally, an altitude controller is designed to calculate the required total thrust  $U_{1d}$  and track  $z_d$ . The desired values of the control inputs are used by the control allocation loop discussed previously.

#### Motion in the $x_l$ - $y_l$ plane

The subsystem  $S_H$  is shown again in (22) for convenience. Being an under-actuated system, there are no exclusive control inputs for motion in the horizon-

tal plane. Hence,  $\bar{u}(\phi, \theta)$  is treated as the control input to  $S_H$ . A backstepping control law is developed to generate the desired roll and pitch angles to maneuver in the  $x_I$ - $y_I$  plane.

$$\begin{aligned}\dot{x}_5 &= x_6 \\ \dot{x}_6 &= g_3 \bar{u}(\phi, \theta)\end{aligned}\tag{22}$$

An error variable  $z_5$  between desired and actual states is defined as

$$z_5 = x_{5d} - x_5\tag{23}$$

A positive definite control Lyapunov function (CLF) [44] in terms of  $z_5$  is given by

$$V(z_5) = \frac{1}{2} z_5^T z_5\tag{24}$$

The time derivative of (24) is given by

$$\dot{V}(z_5) = z_5^T (\dot{x}_{5d} - x_6)\tag{25}$$

Assuming  $x_6$  to be the control input for the subsystem  $\dot{x}_5 = x_6$ , the control law can be written as

$$x_6 = \dot{x}_{5d} + A_5 z_5\tag{26}$$

where  $A_5 \in \mathbb{R}^{2 \times 2}$  is a positive definite diagonal matrix. However,  $x_6$  is actually a system state and not a control input. In any case, its desired value can be set as  $x_{6d} = \dot{x}_{5d} + A_5 z_5$ , and design control  $\bar{u}$  such that  $x_6$  tracks  $x_{6d}$  without any error. Error  $z_6$  between  $x_6$  and  $x_{6d}$  is defined as

$$\begin{aligned}z_6 &= x_{6d} - x_6 \\ z_6 &= \dot{x}_{5d} + A_5 z_5 - x_6\end{aligned}\tag{27}$$

Next, define the augmented CLF as

$$V_a(z_5, z_6) = \frac{1}{2} z_5^T z_5 + \frac{1}{2} z_6^T z_6\tag{28}$$

The time derivative is given by

$$\dot{V}_a(z_5, z_6) = z_6^T (\ddot{x}_{5d} + A_5(z_6 - A_5 z_5)) - z_6^T (g_3 \bar{u}) + z_5^T z_6 - z_5^T A_5 z_5\tag{29}$$

The expression for control  $\bar{u}(\phi, \theta)$  is given by

$$\bar{u}(\phi, \theta) = g_3^{-1}(z_5 + \ddot{x}_{5d} + A_5(z_6 - A_5 z_5) + A_6 z_6) \quad (30)$$

where  $A_6 \in \mathbb{R}^{2 \times 2}$  is a positive definite diagonal matrix. The expression for  $\dot{V}_a$  now becomes

$$\dot{V}_a = -z_5^T A_5 z_5 - z_6^T A_6 z_6 \quad (31)$$

which is negative definite. Existence of  $g_3^{-1}$  was discussed in *Remark 1*. The closed-loop horizontal dynamics is globally exponentially stable. This is shown by substituting (30) in (21), which gives

$$\ddot{z}_5 + (A_6 + A_5)\dot{z}_5 + (I_2 + A_6 A_5)z_5 = 0 \quad (32)$$

Here,  $I_n$  is an identity matrix of size  $n \times n$ . As mentioned above,  $A_5$  and  $A_6$  are diagonal. This implies that the vector equation (32) can be decoupled which results in

$$\ddot{z}_{5j} + (A_{6j} + A_{5j})\dot{z}_{5j} + (1 + A_{6j} A_{5j})z_{5j} = 0 \quad (33)$$

where  $z_{5j}$  is the  $j^{th}$  element of the error vector  $z_5$ ,  $A_{5j}$  is the  $j^{th}$  diagonal element of the gain matrix  $A_5$ , and  $A_{6j}$  is the  $j^{th}$  diagonal element of the gain matrix  $A_6$ . The gain matrices can be chosen such that the condition  $((A_{6j} + A_{5j})^2 - 4(1 + A_{6j} A_{5j})) \geq 0$  is satisfied. This ensures that the stable second order dynamics in (33) has negative real roots that results in the closed-loop dynamics being over-damped or critically damped.

From (21), it is seen that the control input  $\bar{u}(\phi, \theta)$  for horizontal dynamics is in terms of roll angle,  $\phi$ , and pitch angle,  $\theta$ . Hence, the control vector  $\bar{u}(\phi, \theta)$  has to be transformed into desired roll and pitch angles. This is given by

$$\begin{aligned} \phi_d &= \sin^{-1}(\bar{u}_1) \\ \theta_d &= \sin^{-1}\left(\frac{\bar{u}_2}{\cos \phi_d}\right) \end{aligned} \quad (34)$$

where  $\bar{u}_i$  is the  $i^{th}$  element of the control vector given in (30). The values of  $\phi_d$  and  $\theta_d$  are restricted to the interval  $(-\frac{\pi}{3}, \frac{\pi}{3})$  for normal flight. This restriction results from the maximum total thrust that can be produced by the vehicle and

is valid for normal and inverted flight modes. The transition between these two modes however requires stricter conditions which are explained in Section 3.4. Note that these stricter conditions are imposed *only* during the transition and relaxed once the flipping maneuver is completed.

The capability of variable-pitch quadrotor to perform inverted flight implies that the desired roll and pitch angles in (34) have to be appropriately modified. This is necessary for maneuvering in the horizontal plane after flipping. When flip is commanded from normal to inverted flight mode, the decision variable  $\gamma$  is set to -1. The new desired roll and pitch angle are given by

$$\begin{aligned}\phi_d^{flip} &= \pi - \sin^{-1}(\bar{u}_1) \\ \theta_d^{flip} &= \gamma \sin^{-1} \left( \frac{\bar{u}_2}{\cos \phi_d} \right)\end{aligned}\quad (35)$$

The values of  $\phi_d^{flip}$  and  $\theta_d^{flip}$  are restricted to the interval  $(-\frac{2\pi}{3}, \frac{2\pi}{3})$  for inverted flight. Hence, depending on the decision variable  $\gamma$ ,  $(\phi_d, \theta_d, \psi_d)$  or  $(\phi_d^{flip}, \theta_d^{flip}, \psi_d)$  is sent as the reference command to the attitude controller. Next, a backstepping control law for the attitude dynamics is developed.

#### *Attitude control*

A backstepping controller for the rotational subsystem,  $S_R$ , is designed in this section. This generates the desired control vector  $U_d = (U_{2d} \ U_{3d} \ U_{4d})^T$  such that desired roll, pitch, and yaw angles are achieved. The error between desired and actual Euler angles is defined as

$$z_1 = x_{1d} - x_1 \quad (36)$$

The corresponding CLF in terms of  $z_1$  is given by

$$V(z_1) = \frac{1}{2} z_1^T z_1 \quad (37)$$

Its time derivative is given by

$$\dot{V}(z_1) = z_1^T (\dot{x}_{1d} - g_0 x_2) \quad (38)$$

Now,  $x_{2d}$  is considered to be a virtual control input and is designed as

$$x_{2d} = g_0^{-1} (\dot{x}_{1d} + A_1 z_1) \quad (39)$$

where  $A_1 \in \mathbb{R}^{3 \times 3}$  is a positive definite diagonal matrix. This virtual control is the desired value of the state  $x_2$ . The function  $g_0$  is invertible, provided  $\det(g_0) = \sec \theta$ , is a finite value. This is ensured by limiting  $\theta_d$  (and hence,  $\theta_d^{flip}$ ) as discussed in the previous section. Assuming that  $x_2$  tracks  $x_{2d}$ , the time derivative of (37) comes out to be

$$\dot{V}(z_1) = -z_1^T A_1 z_1 \quad (40)$$

This ensures negative definiteness of  $\dot{V}(z_1)$  and renders the error dynamics in  $z_1$  stable. Next,  $z_2$  is defined as the error between actual state  $x_2$  and  $x_{2d}$ . This definition, along with (39), gives

$$g_0 z_2 = \dot{x}_{1d} + A_1 z_1 - g_0 x_2 \quad (41)$$

Define an augmented Lyapunov function  $V_a(z_1, z_2)$  as

$$V_a(z_1, z_2) = \frac{1}{2} z_1^T z_1 + \frac{1}{2} z_2^T z_2 \quad (42)$$

The time derivative along the trajectory of (19) is found to be

$$\dot{V}_a(z_1, z_2) = z_2^T (\dot{x}_{2d}) - z_2^T (f_1 + g_1 U_d) + z_1^T g_0 z_2 - z_1^T A_1 z_1 \quad (43)$$

Vector  $U_d$  is now derived such that  $\dot{V}_a(z_1, z_2)$  is negative definite. Therefore,  $U_d$  is given by

$$U_d = g_1^{-1} (g_0^T z_1 - f_1 + \dot{x}_{2d} + A_2 z_2) \quad (44)$$

where  $A_2 \in \mathbb{R}^{3 \times 3}$  is a positive definite diagonal matrix. The expression for  $\dot{x}_{2d}$  can be derived by differentiating (39). As mentioned in *Remark 1*,  $g_0^{-1}$  and  $g_1^{-1}$  exist. The expression for  $\dot{x}_{2d}$  is derived by differentiating (39) and is given by

$$\dot{x}_{2d} = \frac{d}{dt} (g_0^{-1}) (\dot{x}_{1d} + A_1 z_1) + g_0^{-1} (\ddot{x}_{1d} + A_1 (\dot{x}_{1d} - g_0 x_2)) \quad (45)$$

The time derivative of  $g_0^{-1}$  is given by

$$\frac{d}{dt} (g_0^{-1}) = \begin{pmatrix} 0 & 0 & -\dot{\theta} \cos \theta \\ 0 & -\dot{\phi} \sin \phi & -\dot{\theta} \sin \phi \sin \theta + \dot{\phi} \cos \phi \cos \theta \\ 0 & -\dot{\phi} \cos \phi & -\dot{\theta} \cos \phi \sin \theta - \dot{\phi} \sin \phi \cos \theta \end{pmatrix} \quad (46)$$

Substituting (44) into (43) gives  $\dot{V}(z_1, z_2) = -z_1^T A_1 z_1 - z_2^T A_2 z_2$ , which is negative definite.

From Lyapunov stability theory, this ensures that the errors  $z_1$  and  $z_2$  decay to zero exponentially. This implies that exponential tracking of any set point of the form  $(\phi_d, \theta_d, \psi_d)$  or  $(\phi_d^{flip}, \theta_d^{flip}, \psi_d)$  is achieved. Hence, this ensures exponential attitude stabilization of the quadrotor.

### *Altitude control*

A backstepping controller is designed in this section for the altitude subsystem,  $S_A$ , to attain the desired altitude  $x_{3d}$ . Stability properties of the developed altitude control law is analyzed in the presence of the saturation present in  $U_1$ . Results are presented separately in a section devoted to flip maneuver analysis to ensure clarity and completeness. Define an error between desired and actual altitude as

$$z_3 = x_{3d} - x_3 \quad (47)$$

The corresponding CLF  $V(z_3)$  is chosen as

$$V(z_3) = \frac{1}{2}z_3^2 \quad (48)$$

The time derivative of (48) is given by

$$\dot{V}(z_3) = z_3(\dot{x}_{3d} - x_4) \quad (49)$$

Now,  $x_{4d}$  is considered to be a virtual control input and is designed as

$$x_{4d} = \dot{x}_{3d} + A_3 z_3, \quad A_3 > 0 \quad (50)$$

Design the desired control input  $U_{1d}$  such that  $x_4$  tracks  $x_{4d}$  without any error. Let  $z_4$  be the error between  $x_4$  and  $x_{4d}$ . Substituting for  $x_{4d}$ , the expression for  $z_4$  becomes

$$z_4 = \dot{x}_{3d} + A_3 z_3 - x_4 \quad (51)$$

Since both  $z_3$  and  $z_4$  are required to be zero, define an augmented CLF as

$$V_a(z_3, z_4) = \frac{1}{2}z_3^2 + \frac{1}{2}z_4^2 \quad (52)$$

Its time derivative is given by

$$\dot{V}_a(z_3, z_4) = z_4(\ddot{x}_{3d} + A_3(z_4 - A_3z_3)) - z_4(f_2 - g_2U_{1d}) + z_3z_4 - A_3z_3^2 \quad (53)$$

Now, the required thrust control input  $U_{1d}$  is set as

$$U_{1d} = -g_2^{-1}(z_3 - f_2 + \dot{x}_{3d} + A_3(z_4 - A_3z_3) + A_4z_4) \quad (54)$$

where  $A_4 > 0$ . Note that  $U_{1d}$  derived in (54) is the desired value of actual control input  $U_1$  given in (10). The control allocation loop introduced in Section 3.1 ensures  $U_1$  matches  $U_{1d}$  at all instants of time.

With the control law designed in (54), the derivative of the augmented CLF becomes  $\dot{V}_a(z_3, z_4) = -A_3z_3^2 - A_4z_4^2$ . Hence,  $\dot{V}_a(z_3, z_4)$  is negative definite and the errors  $z_3, z_4$  decay to zero exponentially. However, the function  $g_2$  is not invertible for all values of  $\phi$  and  $\theta$ . It was previously seen that  $\theta$  is restricted to ensure existence of  $g_0^{-1}$ . Now,  $g_2^{-1} \rightarrow \infty$  as  $\cos \phi \rightarrow 0$ . This is neither practically attainable nor numerically feasible for any control signal and occurs exclusively during the flip maneuver. Rotary UAVs are designed such that the maximum thrust produced is twice their weight. Hence, it is logical to impose a saturation on the magnitude of control input  $U_1$  to  $2mg$ .

Such a limit on  $U_1$  results in a set of roll angles for which altitude control is lost during the transition from normal to inverted flight and vice versa. The control law derived in (54) is exponentially stable for all the values of  $\phi$  outside this set. To make the analysis complete, a separate section on the flip maneuver is presented next which explains in detail the time interval as well as the set of roll angles for which altitude control is lost.

### 3.4. The Flip Maneuver

The flip maneuver case is special to variable-pitch quadrotors. During the transition from normal mode to inverted mode and vice versa, the pitch angle  $\theta$  is maintained at values where  $\sin \theta \approx \theta$  holds by suitably restricting the desired pitch angle  $\theta_d$ . Note that the stricter condition on  $\theta$  is imposed only during flipping to ensure that the transition occurs within a finite time interval.

This does not change the already established stability properties of the attitude control law given by (44). The quadrotor inverts by rolling about its  $x_b$ -axis and continues to remain in the inverted state till the decision variable  $\gamma$  is changed back from -1 to 1. During this maneuver, the vehicle passes through a brief phase where altitude control is lost. The altitude control is regained once it enters the inverted mode. Through the following theorems, it is shown that the height lost during the transition is finite and hence, establishing a way to compute the minimum height at which the flip maneuver can be performed. *Theorem 1* shows that for a given input saturation, altitude control is lost for a particular region of the flight envelope during transition from normal to inverted mode and back. However, altitude control is regained within a finite time. *Theorem 2* shows that the time interval for which altitude control is lost can be calculated by decoupling the roll dynamics and computing its settling time for a step change.

**Theorem 1.** *Assuming that  $\sin \theta \approx \theta$  holds throughout the flip maneuver, for a given input saturation of  $2mg$  for the total thrust  $U_1$ , the region of the flight envelope where altitude control is lost during flipping is given by  $\phi \in [-\frac{2\pi}{3}, -\frac{\pi}{3}] \cup [\frac{\pi}{3}, \frac{2\pi}{3}]$ .*

*Proof.* The subsystem  $S_A$  with  $U_1 = \pm 2mg$  and  $\cos \theta \approx 1$  can be expressed as

$$\begin{aligned}\dot{x}_3 &= x_4 \\ \dot{x}_4 &= g \mp 2g \cos \phi\end{aligned}\tag{55}$$

From (55), it is observed that zero acceleration or a net downward acceleration (along positive  $z_I$ -axis, see Fig. 1) if  $g \mp 2g \cos \phi \geq 0$ . The set of roll angles for which this inequality holds can be derived as follows. At  $\cos \phi = \pm \frac{1}{2}$ ,  $\dot{x}_4 = 0$  which implies the desired altitude cannot be tracked and the quadrotor either remains in a state of hover or drifts at a constant velocity along  $z_I$ -axis. For all values of  $\phi$  in the interval  $(-\frac{2\pi}{3}, -\frac{\pi}{3}) \cup (\frac{\pi}{3}, \frac{2\pi}{3})$ , the inequality

$$|\cos \phi| < \frac{1}{2} \implies g \mp 2g \cos \phi > 0$$

holds true. From this, the range of values of  $\phi$  for which altitude control is lost is given by  $\phi \in [-\frac{2\pi}{3}, -\frac{\pi}{3}] \cup [\frac{\pi}{3}, \frac{2\pi}{3}]$ .  $\square$

Hence, the bound for control input  $U_1$  along with the corresponding values for  $\phi$  is given by

$$U_1 = \begin{cases} U_1, & \text{for } \phi \in \left(-\frac{\pi}{3}, \frac{\pi}{3}\right) \cup \left(-\frac{2\pi}{3}, \frac{2\pi}{3}\right) \\ 2mg, & \text{for } \phi \in \left[-\frac{2\pi}{3}, -\frac{\pi}{3}\right] \cup \left[\frac{\pi}{3}, \frac{2\pi}{3}\right] \end{cases}$$

While tracking a trajectory in the horizontal plane in either normal or inverted mode, a restriction on  $\phi_d$  is hence necessary to ensure that altitude control is not lost.

To explicitly compute the time interval for which altitude control is lost, the settling time of the roll subsystem is calculated for a step change in  $\phi$ . This analysis is not required for a conventional quadrotor and has not been presented for a variable-pitch quadrotor in existing literature. Before discussing the theorem, the following considerations must be taken into account:

- (i) The condition  $\sin \theta \approx \theta$  holds during the transition from normal mode to inverted mode and vice versa.
- (ii) The errors  $(\theta_d - \theta)$  and  $(\psi_d - \psi)$  decay to zero exponentially by virtue of the control law given in (44).
- (iii) The gain matrices  $A_1, A_2$  are given by  $A_1 = \text{diag}({}^1a_1, {}^1a_2, {}^1a_3)$  and  $A_2 = \text{diag}({}^2a_1, {}^2a_2, {}^2a_3)$ , where  ${}^1a_1, {}^1a_2, {}^1a_3, {}^2a_1, {}^2a_2, {}^2a_3 > 0$ .

**Theorem 2.** *The time interval for which altitude control is lost during transition between normal and inverted modes, under the condition that  $\sin \theta \approx \theta$  holds during the flip maneuver, is given by  $T_s = \frac{8}{K_1 - \sqrt{K_1^2 - 4K_2}}$ , where  $K_1 = ({}^2a_1 + {}^1a_1)$  and  $K_2 = (1 + {}^2a_1^1 a_1)$ .*

*Proof.* Using the considerations stated above along with the control law in (44), the closed-loop roll dynamics is given by

$$\begin{aligned} \dot{\phi} &= p \\ \dot{p} &= z_\phi + {}^1a_1 \dot{z}_\phi - {}^2a_1 p + {}^2a_1^1 a_1 z_\phi \end{aligned} \tag{56}$$

where  $z_\phi = \phi_d - \phi$  is the roll angle error and  $\dot{x}_{1d}, \ddot{x}_{1d} = 0$ . Hence, the closed-loop

roll error dynamics can be written as

$$\begin{aligned} \ddot{z}_\phi + (^2a_1 + ^1a_1)\dot{z}_\phi + (1 + ^2a_1^1a_1)z_\phi &= 0 \\ \implies \ddot{z}_\phi + K_1\dot{z}_\phi + K_2z_\phi &= 0 \end{aligned} \tag{57}$$

where  $K_1, K_2 > 0$ . Clearly, (57) represents stable second order dynamics in terms of roll error  $z_\phi$ . The dominant (slower) time constant,  $\tau_d$ , for the given over-damped system is given by

$$\tau_d = \frac{2}{K_1 - \sqrt{K_1^2 - 4K_2}}$$

The corresponding settling time for a tolerance of  $\pm 2\%$  is given by

$$T_s = 4\tau_d \tag{58}$$

Considering a step change in  $\phi$  when altitude control is lost, the time taken to regain altitude control is hence given by  $T_s$ .  $\square$

Thus, by choosing appropriate gain matrices  $A_1, A_2$  and effectively deciding the roots of (57), it can be guaranteed that  $z_\phi$  decays to zero with a settling time of  $T_s$ . The terms  $K_1$  and  $K_2$  are chosen to ensure a critically damped or over-damped response. This can now be used to compute the amount of altitude loss in the region  $\phi \in [-\frac{2\pi}{3}, -\frac{\pi}{3}] \cup [\frac{\pi}{3}, \frac{2\pi}{3}]$ .

When there is a transition from normal mode to inverted mode or vice versa, the roll angle  $\phi$  cannot be restricted to interval where the altitude controller is exponentially stable. It has already been established that for  $\phi \in [-\frac{2\pi}{3}, -\frac{\pi}{3}] \cup [\frac{\pi}{3}, \frac{2\pi}{3}]$ , altitude control is lost for the given saturation in  $U_1$ . This results in a net acceleration along the positive  $z_I$ -axis (downward) during the flip maneuver. Note that this downward acceleration occurs only during the transition. From *Theorem 2*, a step change of  $\frac{\pi}{3}$  in  $\phi$  when altitude control is lost occurs within  $T_s$ . The change in height in this region of the flight envelope is determined by the dynamics (55) for  $\phi = \frac{\pi}{3} \rightarrow \phi = \frac{2\pi}{3}$  or  $\phi = -\frac{2\pi}{3} \rightarrow \phi = -\frac{\pi}{3}$ . This can be computed using numerical methods and simulations for the same are shown in later sections. Once this change in roll angle happens, altitude control is regained and the desired height is tracked by the proposed controller.

### 3.5. Gain Allocation

The gain matrices  $A_1, \dots, A_6$  for backstepping control have to be chosen in such a way that the attitude and altitude controllers have a settling time that is at least 5-10 times lesser than the time interval at which the position controller for the horizontal plane dynamics generates roll and pitch set points. This is essential to ensure stability of the complete cascaded system.

Consider the Lyapunov function in (42). After applying the control law given in (44), its time derivative is given by

$$\dot{V}(z_1, z_2) = -z_1^T A_1 z_1 - z_2^T A_2 z_2 \quad (59)$$

Let  $\alpha_1$  be the minimum eigenvalue of the matrix  $A_1$ ,  $\alpha_2$  be the minimum eigenvalue of matrix  $A_2$ ,  $\alpha_5$  be the minimum eigenvalue of matrix  $A_5$ , and  $\alpha_6$  be the minimum eigenvalue of matrix  $A_6$ . The dynamics in (59) can be rewritten as

$$\dot{V}(z_1, z_2) \leq -\sigma V(z_1, z_2) \quad (60)$$

where  $\sigma = \min(\alpha_1, \alpha_2)$ . This implies that (60) is exponentially stable and the errors  $z_1, z_2$  decay to zero at a rate greater than or equal to  $\sigma/2$ . Similarly, the errors  $z_3, z_4$  decay to zero at a rate greater than or equal to  $\frac{1}{2} \min(A_3, A_4)$  and errors  $z_5, z_6$  decay to zero at a rate greater than or equal to  $\frac{1}{2} \min(\alpha_5, \alpha_6)$ . From (15), the error between desired control,  $U_{id}$ , and actual control,  $U_i$ , decays to zero at a rate equal to  $k_i$ . To ensure that the control allocation loop achieves steady state at least 5-10 times faster than the intermediate (attitude and altitude) loop, the condition  $\max(\alpha_1, \alpha_2, A_3, A_4) < \frac{1}{S} \min(k_i)$ , for  $i = 1, 2, 3, 4$ , has to be satisfied. Here,  $S$  is any real value between 5 to 10. Similarly, it has to be ensured that the condition  $\max(\alpha_5, \alpha_6) < \frac{1}{S} \min(\alpha_1, \alpha_2)$  is also satisfied.

### 3.6. Robust Backstepping Control

To ensure that the tracking errors remain uniformly bounded, robust backstepping control laws are proposed. The first order dynamics of the control allocation loop cannot be ignored since it plays an important role in choosing

controller gains to ensure stability of the full system. Hence, the robust controller gains are chosen to be identical to those of the nominal backstepping control laws.

**Theorem 3.** *For the subsystem in (20), with bounded uncertainties and disturbances,  $\Delta_R$ , and the control law given by*

$$U_d = g_1^{-1} (g_0^T z_1 - f_1 + \dot{x}_{2d} + A_2 z_2 + \mu_R) \quad (61)$$

with

$$\mu_R = -\frac{\delta_R^2 z_2}{\delta_R \|z_2\| + \epsilon_R} \quad (62)$$

where  $\mu_R \in \mathbb{R}^3$ ,  $\epsilon_R > 0$ , and  $\|\cdot\|$  is the 2-norm defined on the Euclidean space of appropriate dimension, the errors  $z_1$ ,  $z_2$  remain uniformly bounded  $\forall t \geq 0$ , and the ultimate error bound is given by

$$\|z_1(t)\|_\infty \leq \max \left\{ \|z_1(0)\|_\infty, \left| \sqrt{\frac{\epsilon_R}{c_R}} \right| \right\}, \quad \|z_2(t)\|_\infty \leq \max \left\{ \|z_2(0)\|_\infty, \left| \sqrt{\frac{\epsilon_R}{c_R}} \right| \right\} \quad (63)$$

where  $c_R = \min\{\alpha_1, \alpha_2\}$ ,  $\alpha_1$  is the minimum eigenvalue of the matrix  $A_1$ , and  $\alpha_2$  is the minimum eigenvalue of matrix  $A_2$ .

*Proof.* Using (36)-(43) and the robust control law given by (61), the time derivative of the augmented Lyapunov function  $V_a(z_1, z_2)$  becomes

$$\dot{V}_a(z_1, z_2) = -z_1^T A_1 z_1 - z_2^T A_2 z_2 + z_2^T (\Delta_R + \mu_R) \quad (64)$$

From (18), the last term on the right hand side of (64) satisfies the inequality

$$z_2^T (\Delta_R + \mu_R) \leq \|z_2\| \delta_R + z_2^T \mu_R \quad (65)$$

From (62), the inequality in (65) becomes

$$z_2^T (\Delta_R + \mu_R) \leq \epsilon_R \frac{\delta_R \|z_2\|}{\delta_R \|z_2\| + \epsilon_R} \leq \epsilon_R \quad (66)$$

This implies

$$\dot{V}_a(z_1, z_2) \leq -z_1^T A_1 z_1 - z_2^T A_2 z_2 + \epsilon_R \leq -c_R (\|z_1\|^2 + \|z_2\|^2) + \epsilon_R \quad (67)$$

The result in (67) shows that whenever  $(\|z_1\|^2 + \|z_2\|^2) \geq \left| \frac{\epsilon_R}{c_R} \right|$ ,  $\dot{V}_a(z_1, z_2)$  is negative definite. Since  $\epsilon_R$  is a finite, real, positive number, it can be concluded that  $\dot{V}_a(z_1, z_2)$  is negative outside the compact set  $\mathcal{K}_R$  defined as [44, Section 2.5]

$$\mathcal{K}_R = \left\{ (z_1 + z_2) : (\|z_1\|^2 + \|z_2\|^2) \leq \left| \frac{\epsilon_R}{c_R} \right| \right\}$$

Using the fact that  $V_a(z_1, z_2)$  is a radially unbounded positive definite function,  $\|z_1(t)\|_\infty, \|z_2(t)\|_\infty$  decrease whenever the errors  $z_1, z_2$  are outside the compact set  $\mathcal{K}_R$ . This proves that  $z_1, z_2$  are globally uniformly bounded and gives the error bounds to be

$$\|z_1(t)\|_\infty \leq \max \left\{ \|z_1(0)\|_\infty, \sqrt{\frac{\epsilon_R}{c_R}} \right\}, \quad \|z_2(t)\|_\infty \leq \max \left\{ \|z_2(0)\|_\infty, \sqrt{\frac{\epsilon_R}{c_R}} \right\}$$

□

**Theorem 4.** *For the subsystem in (20), with bounded uncertainties and disturbances,  $\Delta_A$ , and the control law given by*

$$U_{1d} = -g_2^{-1} (z_3 - f_2 + \ddot{x}_{3d} + A_3(z_4 - A_3 z_3) + A_4 z_4 + \mu_A) \quad (68)$$

with

$$\mu_A = -\frac{\delta_A^2 z_4}{\delta_A \|z_4\| + \epsilon_A} \quad (69)$$

where  $\mu_A \in \mathbb{R}$  and  $\epsilon_A > 0$ , the errors  $z_3, z_4$  remain uniformly bounded  $\forall t \geq 0$ , and the ultimate error bound is given by

$$\|z_3(t)\|_\infty \leq \max \left\{ \|z_3(0)\|_\infty, \sqrt{\frac{\epsilon_A}{c_A}} \right\}, \quad \|z_4(t)\|_\infty \leq \max \left\{ \|z_4(0)\|_\infty, \sqrt{\frac{\epsilon_A}{c_A}} \right\} \quad (70)$$

where  $c_A = \min\{A_3, A_4\}$ .

*Proof.* Using (47)-(53) and the robust altitude control law given by (68), the expression for  $\dot{V}_a(z_3, z_4)$  turns out to be

$$\dot{V}_a(z_3, z_4) = -A_3 z_3^2 - A_4 z_4^2 + z_4(\Delta_A + \mu_A) \quad (71)$$

Following steps similar to the proof of Theorem 3, the condition  $\dot{V}_a(z_3, z_4) \leq -c_A(z_3^2 + z_4^2) + \epsilon_A$  is obtained. The compact set outside which  $\dot{V}_a(z_3, z_4)$  is

negative is given by

$$\mathcal{K}_A = \left\{ (z_3 + z_4) : (z_3^2 + z_4^2) \leq \left| \frac{\epsilon_A}{c_A} \right| \right\}$$

Hence, the altitude errors are uniformly ultimately bounded with the bounds given by (70).  $\square$

Note that  $U_{1d}$  designed in (68) also has a maximum value of  $2mg$  and the results from Theorem 1 hold here as well.

**Theorem 5.** *For the subsystem in (21), with bounded uncertainties and disturbances,  $\Delta_H$ , and the control law given by*

$$\bar{u}(\phi, \theta) = g_3^{-1} (z_5 + \ddot{x}_{5d} + A_5(z_6 - A_5 z_5) + A_6 z_6 + \mu_H) \quad (72)$$

with

$$\mu_H = - \frac{\delta_H^2 z_6}{\delta_H \|z_6\| + \epsilon_H} \quad (73)$$

where  $\mu_H \in \mathbb{R}^2$  and  $\epsilon_H > 0$ , the errors  $z_5, z_6$  remain uniformly bounded  $\forall t \geq 0$ , and the ultimate error bound is given by

$$\|z_5(t)\|_\infty \leq \max \left\{ \|z_5(0)\|_\infty, \left| \sqrt{\frac{\epsilon_H}{c_H}} \right| \right\}, \quad \|z_6(t)\|_\infty \leq \max \left\{ \|z_6(0)\|_\infty, \left| \sqrt{\frac{\epsilon_H}{c_H}} \right| \right\} \quad (74)$$

where  $c_H = \min\{\alpha_5, \alpha_6\}$ ,  $\alpha_5$  is the minimum eigenvalue of the matrix  $A_5$ , and  $\alpha_6$  is the minimum eigenvalue of matrix  $A_6$ .

*Proof.* From (23)-(29) and the robust position control law given by (72), the time derivative of  $V_a(z_5, z_6)$  becomes

$$\dot{V}_a(z_5, z_6) = -z_5^T A_5 z_5 - z_6^T A_6 z_6 + z_6^T (\Delta_H + \mu_H) \quad (75)$$

It can be proved that the errors  $z_5, z_6$  are uniformly ultimately bounded with the bounds given by (74) following steps similar to the proofs for Theorems 3 and 4.  $\square$

Using (34), (35), the values of  $\phi_d$ ,  $\theta_d$ ,  $\phi_d^{flip}$ , and  $\theta_d^{flip}$  are computed and supplied to the robust attitude control law in (61).

#### 4. Simulation Results

Before the results for control design of variable-pitch quadrotor system are presented, the aerodynamic behavior of the quadrotor being used is studied using the in-house BEMT analysis with Prandtl's tip loss function. This is used to predict the performance of the variable-pitch rotor system [45]. Figure 2(a) shows the variation of the thrust with blade pitch angle. It is observed that for the given all up weight of 1.2 kg, each rotor needs to generate 300 grams of thrust, which is generated at approximately  $17^\circ$  pitch angle and the corresponding coefficient of thrust is 0.017 as shown in Fig 2(b). It should be noted that the rotor is operating at a relatively high thrust coefficient due to a high all up weight but the rotor is not stalled and the quadrotor is able to fly and maneuver reasonably well. Further, at a pitch angle of  $19^\circ$  the rotor generates a thrust coefficient of 0.02 which is found to be adequate to perform various maneuvers during both simulations and experiments.

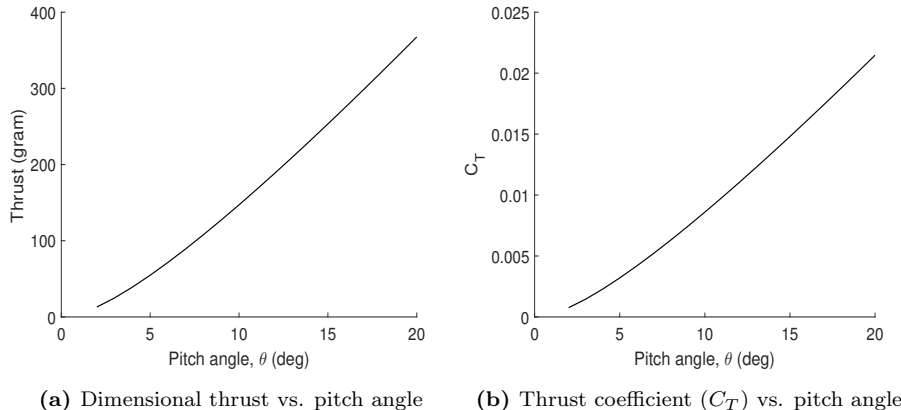


**Figure 2:** Simulated thrust and thrust coefficient variation with pitch angle for rectangular rotor blades of variable-pitch quadrotor with parameters given in Table 1

Figure 3 shows that at a hover throttle of 60 % given manually via radio control (mode 2), the blade pitch angle is measured to be  $17.1^\circ$ . This validates the discussion on aerodynamic behavior of each rotor.



**Figure 3:** Pitch gauge indicating the collective blade pitch angle at 60 % throttle

A performance comparison of the proposed robust backstepping control law and PID in the presence of disturbances is shown through simulations for sinusoidal roll angle tracking as well as sinusoidal tracking in x, y, and z directions in the inertial frame of reference. Since the attitude controller used by default in the PX4 flight stack has a cascaded PID structure and uses geometric methods [46], the default attitude control law is replaced with traditional PID using Euler angles in simulations and experiments for comparison. Numerical simulations of the model as well as controllers are carried out on Matlab. The bounded uncertainties and disturbances in (19)-(21) considered for simulations are given as follows:

$$\Delta_R = \begin{bmatrix} 0.05 \sin(10\pi t) & 0.05 \sin(2\pi t) & 0.05 \sin(4\pi t) \end{bmatrix}^T \text{ N m}$$

$$\Delta_A = 0.01 \sin(8\pi t) \text{ m s}^{-2}$$

$$\Delta_H = \begin{bmatrix} (0.005 \sin(2\pi t) + 0.01) & 0.01 \sin(4\pi t) \end{bmatrix}^T \text{ m s}^{-2}$$

The upper bounds for the uncertainties and disturbances are taken to be  $\delta_R = 0.5$ ,  $\delta_A = 0.15$ , and  $\delta_H = 0.3$ , with  $\epsilon_R = 0.1$  and  $\epsilon_A = \epsilon_H = 0.05$ . This is also validated experimentally and results for the same are included in the next section. To show the effectiveness of the robust controller when performing aerobatic maneuvers, a flipping maneuver to achieve an inverted state is simu-

**Table 1:** Parameters of the variable-pitch quadrotor used for both simulations and experiments

Parameter Name	Value
Mass, $m$	1.2 kg
Radius of rotor blades, $R$	0.145 m
Chord length of blades, $c$	0.030 m
Distance between rotor axis and cg, $d$	0.3 m
Slope of airfoil lift curve, $C_{l_\alpha}$	5.73 rad $^{-1}$
Number of blades per rotor, $N_b$	2
Rotational speed, $\Omega$	3000 rpm
Moment of inertia about $x_b$ , $I_{xx}$	$7.0 \times 10^{-3}$ kg m $^2$
Moment of inertia about $y_b$ , $I_{yy}$	$7.3 \times 10^{-3}$ kg m $^2$
Moment of inertia about $z_b$ , $I_{zz}$	$3.3 \times 10^{-2}$ kg m $^2$

lated numerically and validated experimentally. Parameters of the variable-pitch quadrotor are given in Table 1.

#### 4.1. Attitude Tracking

To demonstrate attitude tracking of the proposed controller, a sinusoid of frequency 1 Hz is given as the reference roll signal. Magnitude of the reference roll sinusoid is 20°. The pitch and yaw angles are stabilized at 0°. Thus, the desired state  $x_{1d}$  supplied to the attitude controller is given by  $x_{1d} = [20 \sin(2\pi t) \ 0 \ 0]^T$ .

The tracking response of the robust attitude controller in comparison to PID is shown in Fig. 4. The gain values for robust backstepping control laws are chosen in accordance with the gain allocation analysis explained previously. The gains also are consistent with the settling time needed to achieve flipping. The backstepping controller gains used for both simulations and experiments are given in Table 2. The gains of the attitude PID controller are chosen as used in the default PX4 flight stack. [The attitude error in the default PX4 flight stack](#)

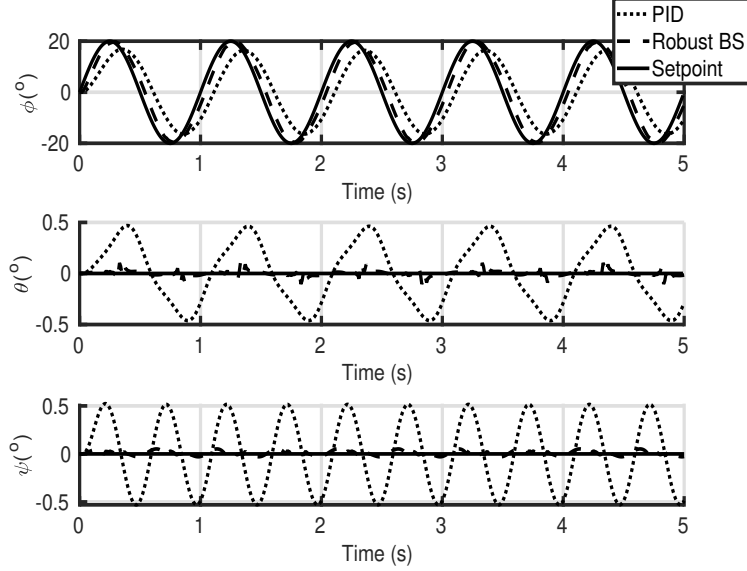


**Figure 4:** Attitude tracking response. Robust backstepping is denoted by “Robust BS”. This naming convention is followed for the forthcoming figures as well.

is derived through geometric methods that use the axis-angle representation. However, the error vector is finally used in a cascaded PID structure [46]. To ensure a fair comparison with Euler angle based PID controllers, the controller proposed in [15] for variable-pitch quadrotors is used here. The gains designed in [15], however, are for robustness to parameter uncertainty. The PID controller performance can be improved by using angular and angular rate gains used in the default PX4 flight stack attitude controller. From Fig. 4 it can be seen that the performance of the robust backstepping control law in the presence of disturbances is better than the PID controller. It can also be seen that the robust controller is able to handle disturbances much better. Disturbances of higher magnitudes cause the performance of the PID controller to deteriorate considerably.

The thrust coefficients and collective pitch angles are computed using the control allocation loop for all three controllers. Their variation with time is shown in Fig. 5(a) and Fig. 5(b), respectively. The PID controller is observed

**Table 2:** Gain values for simulations and experimental flights

$A_1$	diag (31.0 31.0 28.0)
$A_2$	diag (7.5 7.5 7.5)
$A_3$	2.80
$A_4$	1.70
$A_5$	diag (1.50 1.50)
$A_6$	diag (1.45 1.45)

to extract higher effort in terms of thrust coefficients as well as collective pitch angles. This is due to the fact that the linear controller is trying to compensate for the higher error but is unable to track fast changing setpoints. This becomes an impediment when trying aggressive maneuvers like flipping.

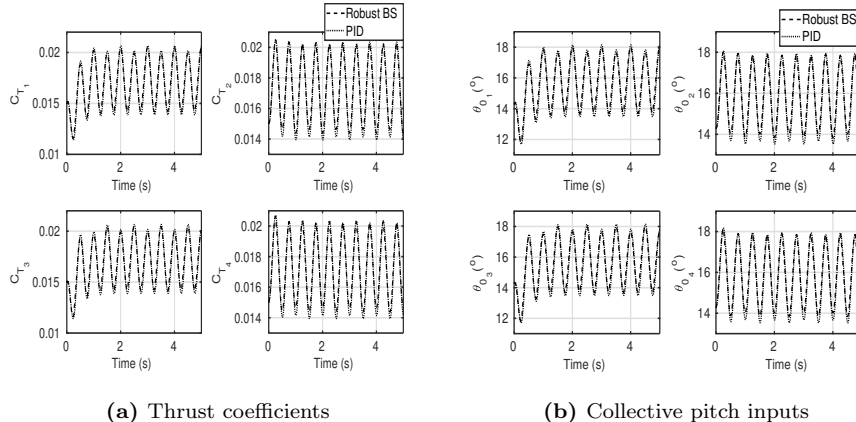


**Figure 5:** Variation of thrust coefficients and blade pitch angles during attitude tracking

#### 4.2. Position Tracking

Performance of the full state robust backstepping controller is demonstrated in the presence of disturbances by tracking sinusoidal trajectories along the  $x_I$ -,  $y_I$ -, and  $z_I$ -axes. The reference trajectories are  $\sin(\frac{\pi}{4}t)$  along the  $x_I$ -axis,  $\cos(\frac{\pi}{4}t)$  along the  $y_I$ -axis, and  $-2 - \sin(\frac{\pi}{4}t)$  along the  $z_I$ -axis. Figure 6 illustrates

the trajectory tracking performance comparison between the proposed robust backstepping controller with a cascaded PID controller [46]. The gains of the position PID controller are chosen as used in the default PX4 flight stack. A slight shift towards the positive  $x_I$ -axis is seen with the shift being highest for the PID controller since there is a constant disturbance in that direction. The error plot in 7(b) shows that the robust backstepping controller is able to track the desired trajectory even in the presence of disturbances with minimal error. The attitude error is shown in 7(a). The desired Euler angle rates,  $\dot{x}_{1d}$ , are taken to be zero for position tracking case. Due to the time scale separation between position and attitude dynamics, the  $\phi_d$  and  $\theta_d$  are assumed to vary slowly enough to treat them as step inputs and thus reduce the attitude tracking problem to a stabilization problem. The commanded yaw angle,  $\psi_d$ , is  $0^\circ$  for all time. It shows that the proposed controller is able to track the commanded sinusoids. The variation of thrust coefficients and collective blade pitch angles during position tracking is shown in Fig. 8.

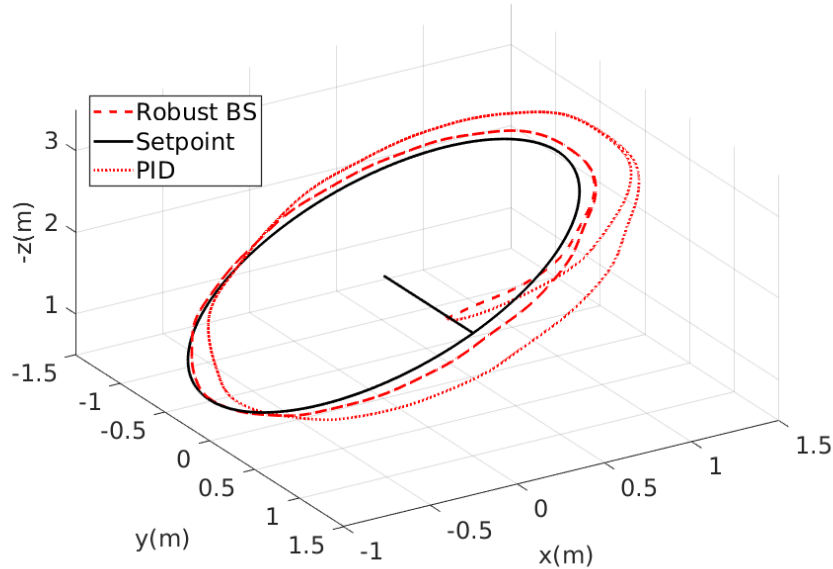


**Figure 6:** Trajectory tracking in 3D

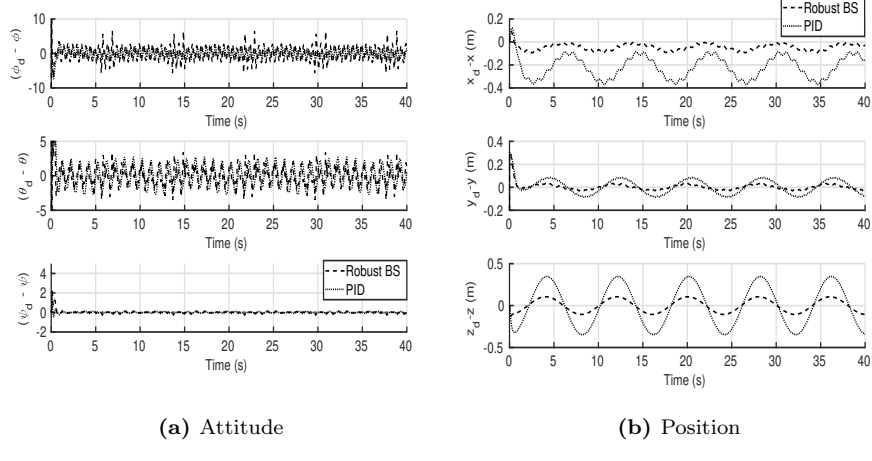


**Figure 7:** Attitude and position errors during sinusoidal trajectory tracking

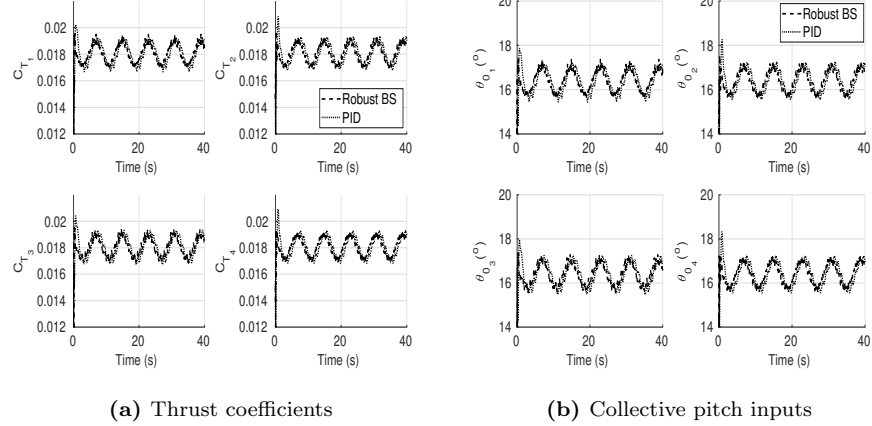


**Figure 8:** Variation of thrust coefficients and blade pitch angles during position tracking

#### 4.3. Flip maneuver

One of the main capabilities of the variable-pitch quadrotor is the ability to reverse its thrust direction. This can be seen while the vehicle performs a flip maneuver in the presence of bounded disturbances. The nonlinear nature of the model as well as the aerodynamic disturbances induced during the aerobatic

maneuver render the PID controller unstable while attempting the flip. Hence, a comparison of the robust and nominal backstepping control is given for the flipping case. Initially, the quadrotor is in a state of hover. The roll, pitch, and yaw angles are at 0 rad. To flip the quadrotor,  $\gamma$  is set to -1 at  $t = 4$ s. This implies that the commanded roll angle changes from  $\phi_d$  to  $\phi_d^{flip} = \pi - \phi_d$ . Time history of attitude is shown in Fig. 9(a). The proposed attitude controller tracks the commanded roll angle without any error. Since the roll angle changes from 0 to  $\pi$  rad ( $180^\circ$ ), there is minimal change in the quadrotor's position as seen in Fig. 9(b). Disturbance rejection is, however, better with the robust backstepping control law as expected.

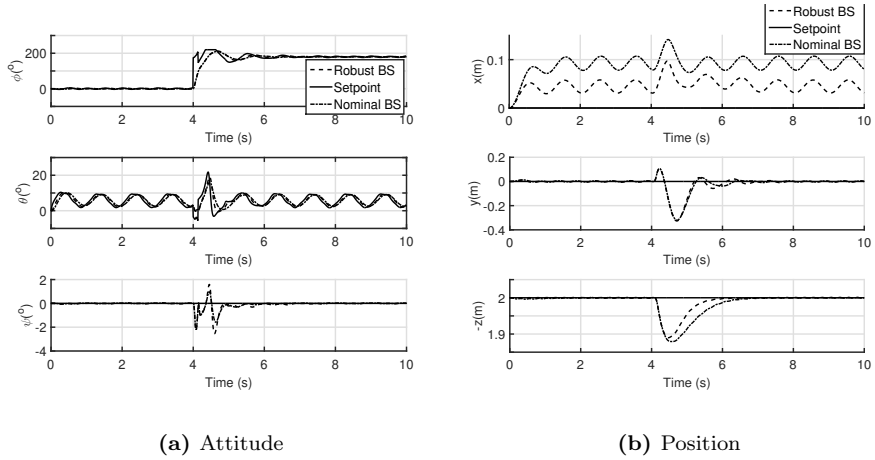


**Figure 9:** Attitude and position variation during flip maneuver. It can be seen that robust backstepping performs better than nominal backstepping in the presence of disturbances.

Trajectory of the quadrotor in the presence of disturbances during this maneuver can be seen in Fig. 10. It is observed that flipping is achieved with a deviation of less than 0.12m in altitude and less than 0.45m along  $y_I$ -axis. The only motion that occurs along  $x_I$ -axis is due to the disturbances. A settling time of  $T_s = 0.53$ s is obtained for the gains given in Table 2. The drop in height when altitude control is lost occurs between  $t = 4.07$ s and  $t = 4.55$ s as observed in 9(b). Hence, the time interval is approximately equal to  $T_s$ . This is consistent

with the flip maneuver stability analysis. The variation of thrust coefficients during the flip maneuver is shown in Fig. 11(a). Collective pitch input to each rotor is calculated using (6). Since thrust is reversed, the collective pitch angle of the blades is also opposite to its initial sign as seen in Fig. 11(b).

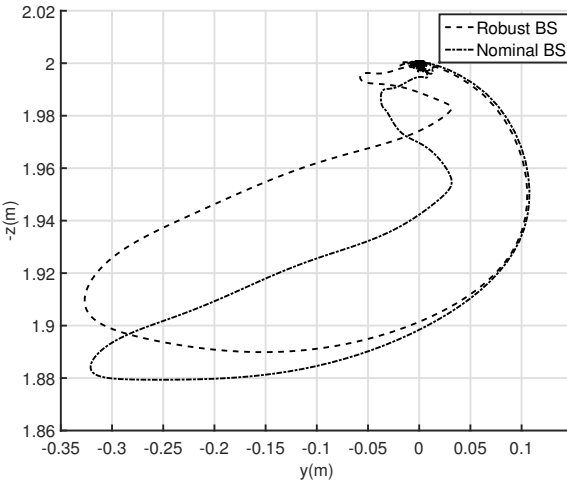


**Figure 10:** Trajectory of the quadrotor during flip maneuver in the  $y_I$ - $z_I$  plane

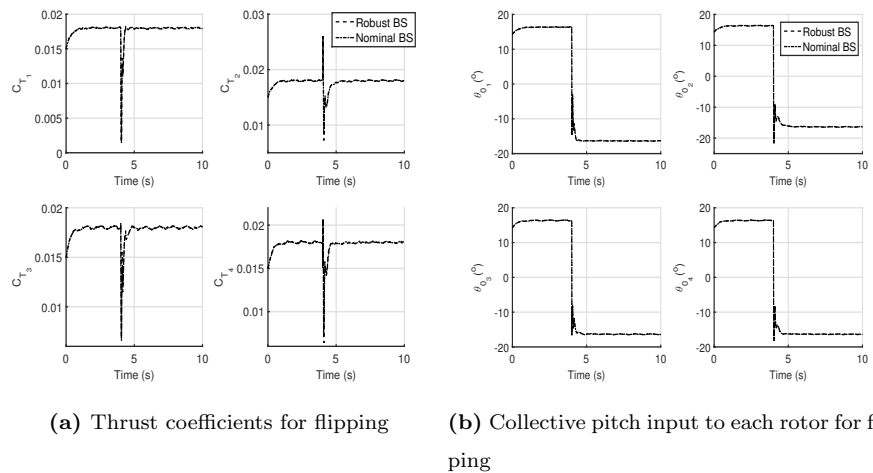


**Figure 11:** Variation of thrust coefficients and blade pitch angles during flip maneuver

## 5. Experimental Results

In this section, the experimental results obtained with the proposed backstepping controller are presented. Details of the setup used are given first. Attitude and position tracking results are then presented for the same desired trajectories used for simulations. Finally, flipping of the quadrotor is shown to demonstrate the capabilities of the developed nonlinear robust control law.

### 5.1. Experimental Setup

A brief description of the vehicle and the associated electronics is given here along with some details about the software (flight stack) used to finally implement the proposed control law.

#### *Hardware Description*

A modified version of a commercial-off-the-shelf (COTS) variable-pitch quadrotor Assault Reaper 500 is used for carrying out experiments (see Fig. 12). It consists of a motor geared to the main drive shaft (gear ratio 14:90) and four rubber belts connected to the shaft that drive the four rotors. The commercial version comes with its own flight controller, radio control transmitter and receiver, and an electronic speed controller (ESC). The aforementioned hardware components are replaced with electronics that are relevant for this work. The ESC used in this set up is Castle Creations Phoenix Edge Lite 75A, 34V ESC with built in 5V battery eliminator circuit (BEC). The ESC is programmed to maintain motor speed at the constant value given in Table 1.

The flight controller used for the experiment is a PixHawk autopilot board by 3D Robotics. It has 8 main outputs out of which 5 are used for this experiment. Four outputs are utilized to send control signals to the four servo motors actuating the blade pitch angles. Since these servos cannot be powered by PixHawk internally, the fifth output is used to connect the BEC present in the ESC. Signals to turn the motor on and off can also be sent through the output that is connected to the ESC. In addition to the autopilot board, a 433MHz telemetry module is used for remote communication between the autopilot and the ground

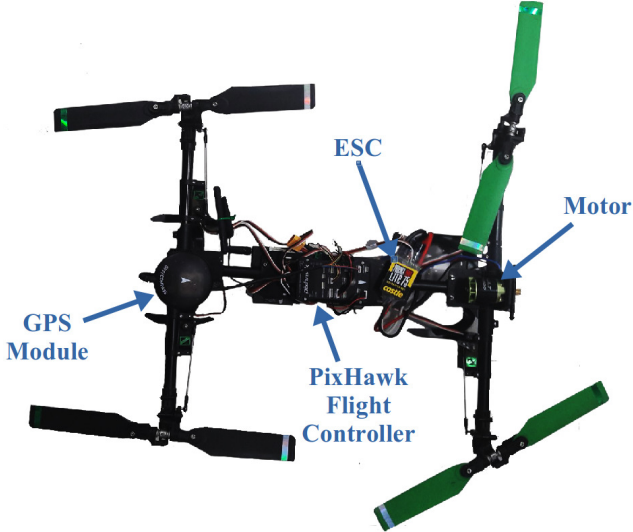


**Figure 12:** Quadrotor used for experiments

station. A FrSky X8R receiver is connected to the PixHawk autopilot to receive manual control inputs (in manual mode) and signals to switch between manual and auto modes. This receiver is paired with a FrSky X9D transmitter which contains the throttle, roll, pitch, and yaw sticks along with mode switches as shown in Fig. 3. A GPS receiver is fixed onboard to provide data for global position feedback.

#### *Software Description*

The PixHawk flight controller comes with a firmware called “PX4 flight stack”. This provides a modular platform and uses a Unix based approach and a bash-like shell. The microcontroller-based execution environment has a low latency and good hardware connectivity. Such a software structure provides us ample scope to experiment with various control laws. The related details can be found in [47].

The flight stack, as mentioned earlier, is modular and hosts controllers for position and attitude, extended Kalman filter (EKF) for state estimation, and drivers for onboard sensors such as IMUs, barometer, compass, and gyroscope.

The modules present for PID control of both position and attitude are completely replaced by our proposed backstepping controller. The EKF module that comes with the PX4 flight stack is utilized to estimate all the required states. All related software resources are open source and can be found in [46]. Parameters of Assault Reaper 500 are assumed to be the same as those used for simulations. The gain matrices  $A_1, \dots, A_6$  are presented in Table 2. For ease of design, these matrices are considered to be diagonal. The servos update at a rate of 250 Hz, which is well above the gain allocation threshold discussed in Section 3 (in terms of frequency rather than settling time).

### *5.2. Flight Results*

This section presents experimental flight results of implementing a nonlinear backstepping control law on the variable-pitch quadrotor described in the previous section. The state estimates from the EKF running onboard the Pixhawk flight controller are plotted to obtain noise-free data.

#### *Attitude Tracking*

Attitude tracking performance of the proposed backstepping controller is validated through experiments. A sinusoidal signal of frequency 1 Hz and magnitude  $20^\circ$  is given as the roll angle reference signal. This is analogous to the simulation analysis done previously. However, manual inputs from the radio controller were enabled for the pitch and yaw channels for safety reasons. The roll tracking response is shown in Fig. 13. The robust backstepping controller shows good tracking performance. The disturbances were minimal during the experiment. However, tracking performance of the PID controller for fast changing signals deteriorate rapidly. The thrust coefficients and collective pitch inputs computed by the controllers are shown in Fig. 14. Note that these are not measurements of the actual blade pitch angles, but the inputs to the actuators. The computed collective pitch angles are normalized between -1 to 1 before converting it into PWM signals that is supplied to the servos.

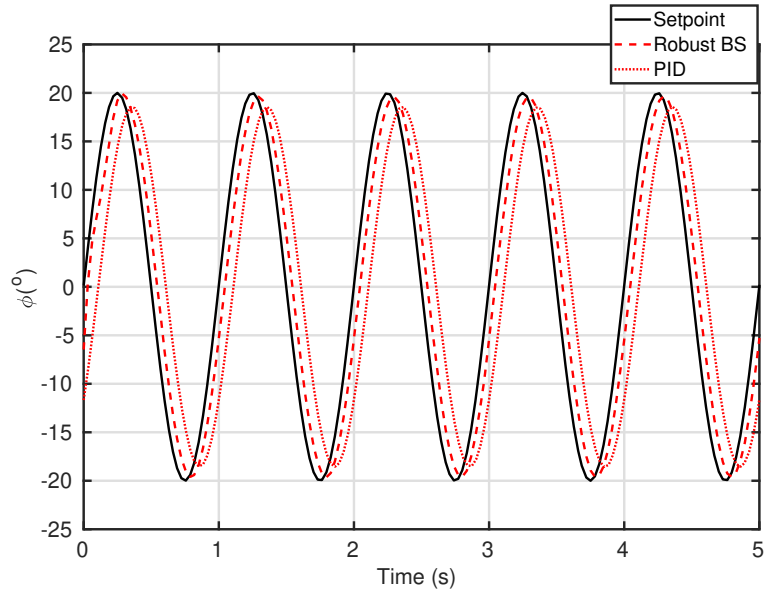
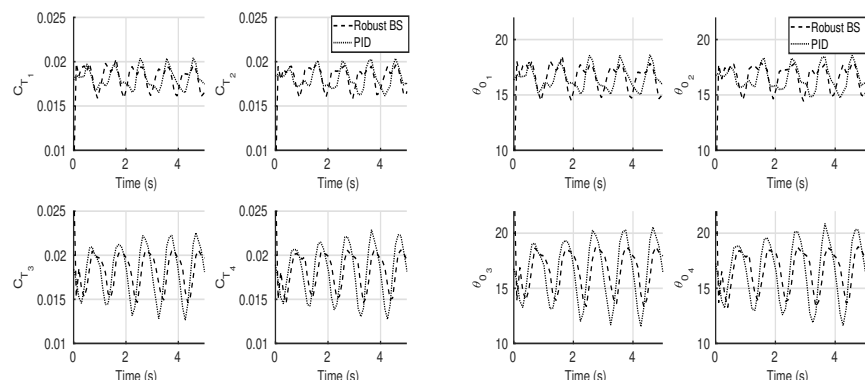


**Figure 13:** Experimental roll tracking with robust backstepping and PID



**(a)** Thrust coefficients for roll tracking experiment  
**(b)** Collective pitch input to each rotor for roll tracking experiment

**Figure 14:** Thrust coefficients and blade pitch angles during experimental roll tracking

### Position Tracking

Sinusoidal trajectories along  $x_I$ -,  $y_I$ -, and  $z_I$ -axes are given as reference trajectories to experimentally validate the robust backstepping control law including a comparison with the default PID controller used in the PX4 flight stack. The reference trajectories are  $\sin(\frac{\pi}{4}t)$  along the  $x_I$ -axis,  $\cos(\frac{\pi}{4}t)$  along the  $y_I$ -axis, and  $-10 - \sin(\frac{\pi}{4}t)$  along the  $z_I$ -axis. These reference signals are identical to those used for simulations except for the mean height. Again, the commanded yaw angle,  $\psi_d$ , is  $0^\circ$  for all time, for all three controllers. The 3D trajectory of the variable-pitch quadrotor is shown along with the reference trajectory in Fig. 15. Variation of position and the corresponding attitude is shown in Fig. 16. It can be observed in Fig. 16(a) that each position controller produces its own roll and pitch angle setpoints. The thrust coefficients and collective pitch inputs computed by the controllers are shown in Fig. 17. Again, note that these are not measurements of the actual blade pitch angles.

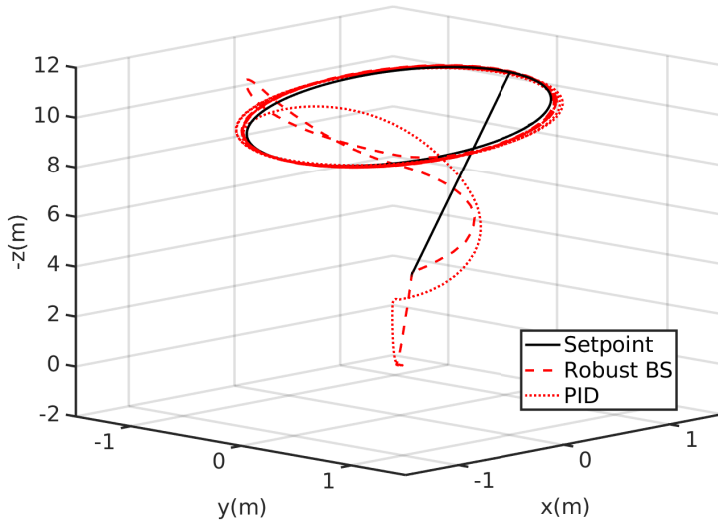
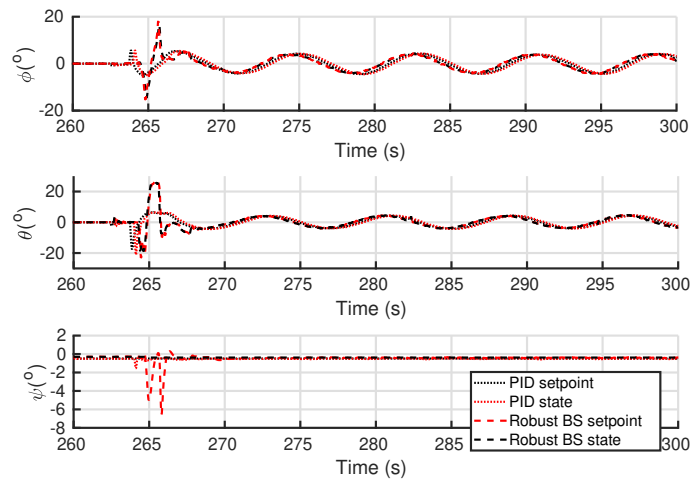
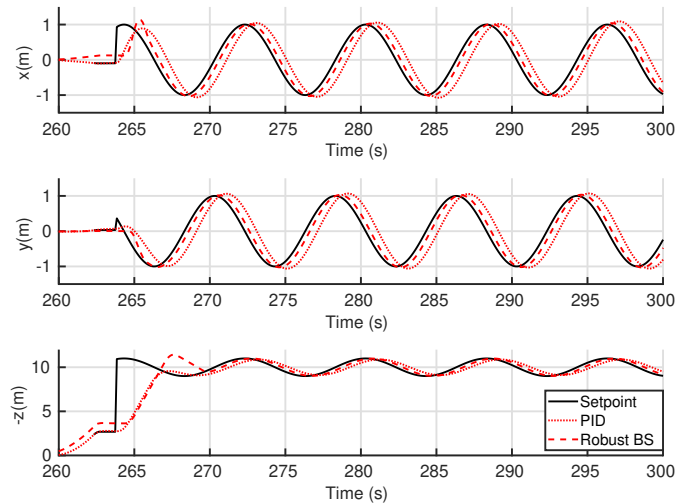


**Figure 15:** Trajectory tracking in 3D using robust backstepping and PID controllers.

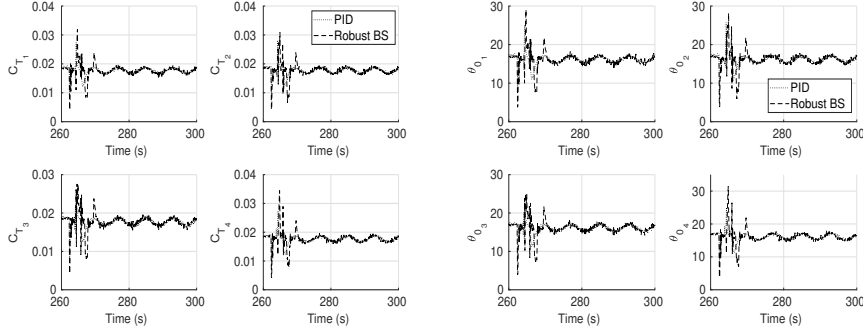


(a) Attitude



(b) Position

**Figure 16:** Attitude and position variation during experimental sinusoidal trajectory tracking



(a) Thrust coefficients for position tracking ex-(b) Collective pitch input to each rotor for po-  
periment

sition tracking experiment

**Figure 17:** Variation of thrust coefficients and blade pitch angles during experimental posi-  
tion tracking

#### *Quadrotor Flipping*

To show the effectiveness of the proposed robust backstepping attitude control law, flipping of the variable-pitch quadrotor is validated experimentally. The roll response is shown in Fig. 18. Since flipping is a stabilization problem,  $\dot{x}_{1d}$  is set to zero. It can be observed that the quadrotor is able to flip within 1s. This shows that the time duration for which the roll angle is in the interval  $\phi \in [-\frac{2\pi}{3}, -\frac{\pi}{3}] \cup [\frac{\pi}{3}, \frac{2\pi}{3}]$  is clearly less than 1s. Hence, a minimal loss in altitude is expected in this time interval. The computed thrust coefficients and blade pitch angles are shown in Fig. 19. To ensure that the quadrotor does not have any upward acceleration while constrained physically (see Fig. 20(a)), the experiments are performed with low collective pitch inputs before and after flipping. The differential thrust produced by actuating rotors 1 and 2 with negative pitch angles and rotors 3 and 4 with positive pitch angles when the flip from normal to inverted state is commanded allows the quadrotor to achieve the aggressive maneuver quickly. The opposite actuation of rotors 1 through 4 is observed for flipping back from inverted to normal state. These actuation signals can be clearly seen in Fig. 19(b). Screen grabs of the video showing the flip experiment conducted at IIT Kanpur are shown in Fig. 20.

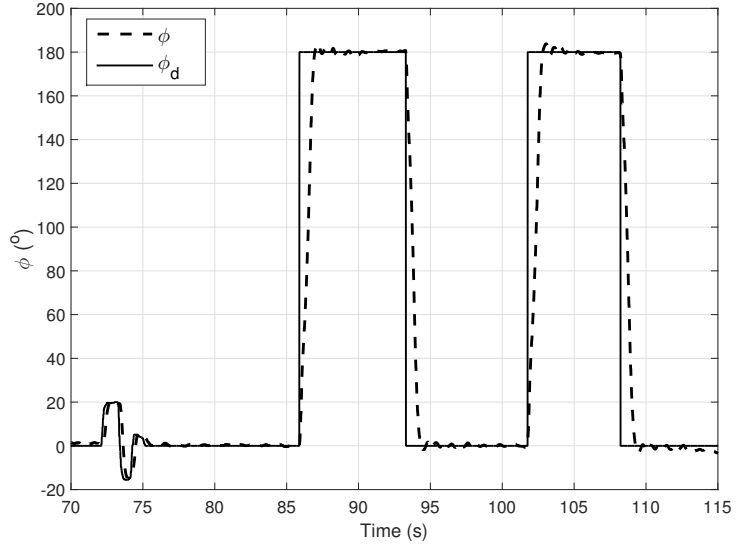
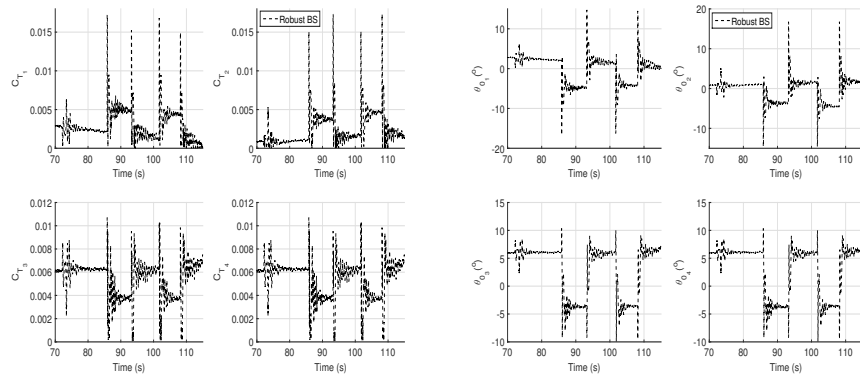


**Figure 18:** Experimental flip maneuver with robust backstepping. The roll angle is seen to change within 1s and the response seen is analogous to that in simulations.



(a) Thrust coefficients for roll tracking experiment  
(b) Collective pitch input to each rotor for roll tracking experiment

**Figure 19:** Variation of thrust coefficients and blade pitch angles during experimental flip. The blade pitch angles have a low value since the quadrotor is physically constrained and an upward acceleration is not desirable or safe.

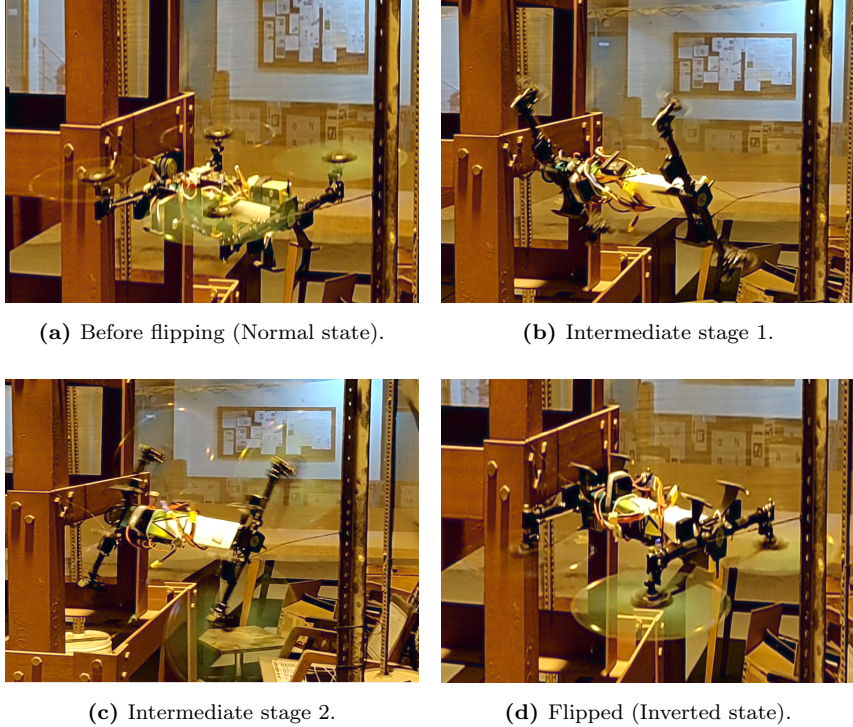


**Figure 20:** Video grabs of the flipping experiment. Video of the experiments can be found at [48].

## 6. Conclusions

This paper discusses the design of nominal and robust nonlinear backstepping controllers for a variable-pitch quadrotor. The full six degrees of freedom model is discussed including the associated rotor dynamics and control inputs. Difficulties in handling the irrational expression for control inputs were overcome by introducing a control allocation loop. Lyapunov theory is utilized to first derive a nominal backstepping controller for the physics model assuming no uncertainties or disturbances. The nominal control law allows systematic selection of controller gains and also analyze stability of the full system in the presence of dynamic control allocation. A comprehensive analysis of the flip maneuver is presented for the first time. Robust nonlinear control design is then proposed to ensure errors remain uniformly bounded in the presence of unmod-

eled dynamics and bounded disturbances. The performance of the proposed controller is demonstrated first through numerical simulations. Experimental validation of attitude and position tracking as well as the flip maneuver is carried out to show the effectiveness of the proposed robust control design.

### Acknowledgements

The authors would like to thank Nidhish Raj, PhD candidate, Dept. of Aerospace Engineering, IIT Kanpur, for his invaluable inputs during the experiments carried out to validate the proposed controller.

### References

- [1] M. Y. Amir, V. Abbass, Modeling of quadrotor helicopter dynamics, International Conference on Smart Manufacturing Application (ICSMA) (2008) 100–105doi:10.1109/ICSMA.2008.4505621.
- [2] S. Bouabdallah, P. Murrieri, R. Siegwart, Design and control of an indoor micro quadrotor, IEEE International Conference on Robotics and Automation (ICRA) 5 (2004) 4393–4398. doi:10.1109/ROBOT.2004.1302409.
- [3] P. Pounds, R. Mahony, P. Corke, Modelling and control of a large quadrotor robot, Control Engineering Practice 18 (7) (2010) 691–699. doi:10.1016/j.conengprac.2010.02.008.
- [4] B. Erginer, E. Altug, Modeling and pd control of a quadrotor vtol vehicle, IEEE Intelligent Vehicles Symposium (2007) 894–899doi:10.1109/IVS.2007.4290230.
- [5] S. Lupashin, A. Schöllig, M. Sherback, R. D’Andrea, A simple learning strategy for high-speed quadrocopter multi-flips, IEEE International Conference on Robotics and Automation (ICRA) (2010) 1642–11648doi:10.1109/ROBOT.2010.5509452.

- [6] D. Mellinger, N. Michael, V. Kumar, Trajectory generation and control for precise aggressive maneuvers with quadrotors, *International Journal of Robotics Research* 31 (5) (2012) 664–674. doi:10.1177/0278364911434236.
- [7] D. Mellinger, V. Kumar, Minimum snap trajectory generation and control for quadrotors, *IEEE International Conference on Robotics and Automation (ICRA)* (2011) 2520–2525doi:10.1109/ICRA.2011.5980409.
- [8] F. Oliva-Palomo, A. Sanchez-Orta, P. Castillo, H. Alazki, Nonlinear ellipsoid based attitude control for aggressive trajectories in a quadrotor: Closed-loop multi-flips implementation, *Control Engineering Practice* 77 (2018) 150–161.
- [9] M. Cutler, N. K. Ure, B. Michini, J. How, Comparison of fixed and variable pitch actuators for agile quadrotors, 2011. doi:10.2514/6.2011-6406.
- [10] M. Cutler, J. How, Actuator constrained trajectory generation and control for variable-pitch quadrotors, 2012. doi:10.2514/6.2012-4777.
- [11] N. Gupta, M. Kothari, Abhishek, Flight dynamics and nonlinear control design for variable-pitch quadrotors, *IEEE American Control Conference (ACC)* (2016) 3150–3155doi:10.1109/ACC.2016.7525402.
- [12] Abhishek, R. Gadekar, A. Duhoon, M. Kothari, S. Kadukar, L. Rane, G. Suryavanshi, Design, development, and closed-loop flight-testing of a single power plant variable pitch quadrotor unmanned air vehicle, *American Helicopter Society Annual Forum*, 2017.
- [13] F. Riccardi, M. Lovera, Robust attitude control for a variable-pitch quadrotor, *IEEE Conference on Control Applications (CCA)* (2014) 730–735doi:10.1109/CCA.2014.6981427.
- [14] E. Fresk, G. Nikolakopoulos, Experimental model derivation and control of a variable pitch propeller equipped quadrotor, *IEEE Conference on Control Applications (CCA)* (2014) 723–729doi:10.1109/CCA.2014.6981426.

- [15] M. Bhargavapuri, S. R. Sahoo, M. Kothari, Abhishek, Robust attitude control in the presence of parameter uncertainty for a variable pitch quadrotor, IEEE American Control Conference (ACC) (2018).
- [16] A. Das, K. Subbarao, F. Lewis, Dynamic inversion with zero-dynamics stabilisation for quadrotor control, IET Control Theory Applications 3 (3) (2009) 303–314. doi:10.1049/iet-cta:20080002.
- [17] A. Benallegue, A. Mokhtari, L. Fridman, Feedback linearization and high order sliding mode observer for a quadrotor uav, IEEE International Workshop on Variable Structure Systems (VSS) (2006) 365–372doi:10.1109/VSS.2006.1644545.
- [18] S. Bouabdallah, R. Siegwart, Full control of a quadrotor, International conference on Intelligent robots and systems (IROS) (2007) 153–158doi:10.1109/IROS.2007.4399042.
- [19] A. Das, F. Lewis, K. Subbarao, Backstepping approach for controlling a quadrotor using lagrange form dynamics, Journal of Intelligent and Robotic Systems 56 (1-2) (2009) 127–151. doi:10.1007/s10846-009-9331-0.
- [20] T. Madani, A. Benallegue, Backstepping control for a quadrotor helicopter, IEEE/RSJ International Conference on Intelligent Robots and Systems (2006) 3255–3260doi:10.1109/IROS.2006.282433.
- [21] A. Nagaty, S. Saeedi, C. Thibault, M. Seto, H. Li, Control and navigation framework for quadrotor helicopters, Journal of intelligent & robotic systems (2013) 1–12.
- [22] R. Hess, M. Bakhtiari-Nejad, Sliding-mode control of a nonlinear model of an unmanned aerial vehicle, Journal of Guidance, Control, and Dynamics 31 (4) (2008) 1163–1166. doi:10.2514/1.32558.
- [23] S. Bouabdallah, R. Siegwart, Backstepping and sliding-mode techniques applied to an indoor micro quadrotor, IEEE International

Conference on Robotics and Automation (ICRA) (2005) 2259–2264doi:10.1109/ROBOT.2005.1570447.

- [24] I. González-Hernández, S. Salazar, A. Rodríguez-Mata, F. Muñoz-Palacios, R. López, R. Lozano, Enhanced robust altitude controller via integral sliding modes approach for a quad-rotor aircraft: Simulations and real-time results, *Journal of Intelligent & Robotic Systems* (2017) 1–15doi:10.1007/s10846-017-0527-4.
- [25] T. Lee, M. Leoky, N. H. McClamroch, Geometric tracking control of a quadrotor uav on se (3), *IEEE International Conference on Decision and Control (CDC)* (2010) 5420–5425doi:10.1109/CDC.2010.5717652.
- [26] Z. T. Dydek, A. M. Annaswamy, E. Lavretsky, Adaptive control of quadrotor uavs: A design trade study with flight evaluations, *IEEE Transactions on Control Systems Technology* 21 (4) (2013) 1400–1406. doi:10.2514/6.2010-7575.
- [27] A. Lanzon, A. Freddi, S. Longhi, Flight control of a quadrotor vehicle subsequent to a rotor failure, *Journal of Guidance, Control, and Dynamics* 37 (2) (2014) 580–591. doi:10.2514/1.59869.
- [28] J.-F. Guerrero-Castellanos, J. J. Téllez-Guzmán, S. Durand, N. Marchand, J. Alvarez-Muñoz, V. R. Gonzalez-Díaz, Attitude stabilization of a quadrotor by means of event-triggered nonlinear control, *Journal of Intelligent & Robotic Systems* 73 (1-4) (2014) 123–135.
- [29] F. Kendoul, D. Lara, I. Fantoni, R. Lozano, Real-time nonlinear embedded control for an autonomous quadrotor helicopter, *Journal of Guidance, Control, and Dynamics* 30 (4) (2007) 1049–1061. doi:10.2514/1.27882.
- [30] H. Liu, D. Li, Z. Zuo, Y. Zhong, Robust attitude control for quadrotors with input time delays, *Control Engineering Practice* 58 (2017) 142–149.

- [31] Y. Yu, Q. Wang, C. Sun, H. Liu, Robust compensator with constraints for attitude manoeuvres of a quadrotor subject to unknown stochastic input delays, *Journal of Control and Decision* (2018) 1–27.
- [32] T. Lee, M. Leok, N. H. McClamroch, Nonlinear robust tracking control of a quadrotor uav on  $\text{se}(3)$ , *Asian Journal of Control* 15 (2) (2013) 391–408.
- [33] N. Raj, R. N. Banavar, M. Kothari, Abhishek, Robust attitude tracking control of aerobatic helicopters: A geometric backstepping approach, arXiv preprint arXiv:1709.05652 (2017).
- [34] W. Liu, Y. Wei, G. Duan, M. Hou, Integrated guidance and control with input saturation and disturbance observer, *Journal of Control and Decision* 5 (3) (2018) 277–299.
- [35] J. Mao, H. R. Karimi, Z. Xiang, Observer-based adaptive consensus for a class of nonlinear multiagent systems, *IEEE Transactions on Systems, Man, and Cybernetics: Systems* (99) (2017) 1–8.
- [36] M. Hongjun, Y. Liu, T. Li, G.-H. Yang, Nonlinear high-gain observer-based diagnosis and compensation for actuators and sensors faults in a quadrotor unmanned aerial vehicle, *IEEE*, 2018.
- [37] H. Wang, H. R. Karimi, P. X. Liu, H. Yang, Adaptive neural control of nonlinear systems with unknown control directions and input dead-zone, *IEEE Transactions on Systems, Man, and Cybernetics: Systems* (99) (2017) 1–11.
- [38] T. Youssef, M. Chadli, H. R. Karimi, R. Wang, Actuator and sensor faults estimation based on proportional integral observer for ts fuzzy model, *Journal of the Franklin Institute* 354 (6) (2017) 2524–2542.
- [39] S. K. Kommuri, M. Defoort, H. R. Karimi, K. C. Veluvolu, A robust observer-based sensor fault-tolerant control for pmsm in electric vehicles, *IEEE Transactions on Industrial Electronics* 63 (12) (2016) 7671–7681.

- [40] R. Rashad, A. Aboudonia, A. El-Badawy, Backstepping trajectory tracking control of a quadrotor with disturbance rejection, International Conference on Information, Communication and Automation Technologies (ICAT) (2015) 1–7doi:10.1109/ICAT.2015.7340523.
- [41] R. W. Beard, T. W. McLain, Small unmanned aircraft: Theory and practice, Princeton university press, 2012.
- [42] J. G. Leishman, Principles of helicopter aerodynamicsCambridge University Press, Chapter 3.
- [43] V. S. Chipade, A. Abhishek, M. Kothari, Advanced flight dynamic modelling of variable pitch quadrotor, in: 2018 AIAA Atmospheric Flight Mechanics Conference, 2018, p. 1763.
- [44] M. Krstic, I. Kanellakopoulos, P. Kokotovic, Nonlinear and adaptive control designWiley, Chapter 2.
- [45] K. Bhatnagar, Abhishek, Effect of rotor blade geometry on the performance of rotary-winged micro air vehicle, Defence Science Journal 66 (6) (2016) 638–644. doi:10.14429/dsj.66.9659.
- [46] Px4 developer guide.  
URL <http://px4.io/>
- [47] L. Meier, D. Honegger, M. Pollefeys, Px4: A node-based multithreaded open source robotics framework for deeply embedded platforms, in: IEEE International Conference on Robotics and Automation (ICRA), 2015, IEEE, 2015, pp. 6235–6240.
- [48] Robust backstepping control experiments on a variable-pitch quadrotor.  
URL <https://www.youtube.com/watch?v=jKorhM1JLLo>